Cell

Terminal Axon Branching Is Regulated by the LKB1-NUAK1 Kinase Pathway via Presynaptic Mitochondrial Capture

Julien Courchet,[1,3] Tommy L. Lewis, Jr.,[1,3] Sohyon Lee,[1] Virginie Courchet,[1] Deng-Yuan Liou,[1] Shinichi Aizawa,[2] and Franck Polleux[1,*]

[1]Dorris Neuroscience Center and Department of Molecular and Cellular Neuroscience, The Scripps Research Institute, La Jolla, CA 92037-1000, USA

[2]RIKEN Institute, 2-2-3 Minatojima-minamimachi, Chuo-ku, Kobe 650-0047, Japan

[3]These authors contributed equally to this work

*Correspondence: polleux@scripps.edu

http://dx.doi.org/10.1016/j.cell.2013.05.021

SUMMARY

The molecular mechanisms underlying the axon arborization of mammalian neurons are poorly understood but are critical for the establishment of functional neural circuits. We identified a pathway defined by two kinases, LKB1 and NUAK1, required for cortical axon branching in vivo. Conditional deletion of LKB1 after axon specification or knockdown of NUAK1 drastically reduced axon branching in vivo, whereas their overexpression was sufficient to increase axon branching. The LKB1-NUAK1 pathway controls mitochondria immobilization in axons. Using manipulation of Syntaphilin, a protein necessary and sufficient to arrest mitochondrial transport specifically in the axon, we demonstrate that the LKB1-NUAK1 kinase pathway regulates axon branching by promoting mitochondria immobilization. Finally, we show that LKB1 and NUAK1 are necessary and sufficient to immobilize mitochondria specifically at nascent presynaptic sites. Our results unravel a link between presynaptic mitochondrial capture and axon branching.

INTRODUCTION

The neocortex forms a complex network composed of billions of interconnected neurons arranged in six layers that are defined by molecular, morphological, and electrophysiological properties and—importantly—by their afferent and efferent inputs. This pattern of connectivity is achieved through tightly regulated developmental processes whose impairments have profound effects on cortical function and are linked to neurodevelopmental defects ranging from epilepsy to mental retardation and autism spectrum disorders (Walsh et al., 2008; Zoghbi and Bear, 2012). In the mouse, the development of cortical pyramidal neurons occurs in three main stages (Barnes and Polleux, 2009; Donahoo and Richards, 2009). First, from approximately embryonic day (E) 11 to E18, neurons are born, engage radial migration, and form a leading process that will eventually become the apical dendrite and a trailing process that becomes the axon. Second, during and after neuronal migration and until approximately postnatal day (P) 7, axons grow and are guided to their proper subcortical or cortical targets by axon guidance cues. Third, during the second and third postnatal weeks, axons branch extensively upon reaching their final targets and form functional synapses with their postsynaptic partners. Important progress has been made in identifying the molecular mechanisms regulating axon growth and guidance (Huber et al., 2003; Polleux and Snider, 2010). However, relatively little is known about the molecular mechanisms controlling terminal axon branching (Gallo, 2011; Hall and Lalli, 2010; Jeanneteau et al., 2010; Kalil et al., 2000), although it is clear that, in many axons, including cortical projections, axon branching is controlled by both activity-independent and activity-dependent mechanisms (Mizuno et al., 2007, 2010; Uesaka et al., 2006; Wang et al., 2007; Yu et al., 2004).

We and others have demonstrated that the serine/threonine kinase LKB1 (liver kinase B1, also called STK11 or Par4) is critical for axon specification during neuronal polarization in vivo (Barnes et al., 2007; Shelly et al., 2007). LKB1 belongs to a family of highly conserved proteins known as the PAR (*Par*tition defective) proteins, initially identified in *C. elegans* as required for the first asymmetric zygotic cell division (Kemphues et al., 1988). It has since been shown to regulate cell polarity in a wide range of cell types and animal models (Watts et al., 2000; Martin and St Johnston, 2003; Baas et al., 2004). By phosphorylating a conserved threonine present in the T loop of their catalytic domains, LKB1 is the "master" activator of 14 downstream kinases, including AMPKα1/α2, SAD-A/B (BRSK2 and BRSK1, respectively), NUAK1/2 (ARK5 and SNARK, respectively), SIK1-3, MARK1-4, and SNRK (Jaleel et al., 2005; Lizcano et al., 2004). AMPK is one of the main metabolic sensors in the cell, and its activity has been linked to the regulation of metabolism and to the maintenance of polarity under stress conditions (Lee et al., 2007; Mirouse et al., 2007). However, we observed that LKB1 is not a major activator of AMPK in neurons (Barnes et al., 2007) and that AMPK is not required for cortical

neuron polarization in vivo (Williams et al., 2011), although its overactivation by metabolic stress impairs axon growth in vitro (Amato et al., 2011; Williams et al., 2011). The biological functions of the other 12 AMPK-like kinases are still largely unknown in vivo (Alessi et al., 2006). LKB1 exerts its function in early axon specification through activation of synapses of amphids defective (SAD)-A/B (Barnes et al., 2007; Kishi et al., 2005), but whether or not LKB1 and other AMPK-like kinases play any role during subsequent steps of neuronal development beyond axon specification remains unknown (Barnes and Polleux, 2009).

RESULTS

Postmitotic Deletion of LKB1 Does Not Impair Neuron Polarization

In our previous study, LKB1 conditional inactivation was performed by crossing mice harboring a floxed allele for *Lkb1* (*LKB1*$^{F/F}$) (Bardeesy et al., 2002) with a mouse line expressing the bacterial Cre-recombinase under the dorsal telencephalon-specific promoter Emx1 (Gorski et al., 2002). Recombination in Emx1^{Cre} mice occurs as early as E10 (Gorski et al., 2002) in radial glial cells (RGC), the main neural progenitors generating all pyramidal neurons in the dorsal telencephalon. In order to determine at what stage of neuron development LKB1 activity is required for axon specification, we used the NEX^{Cre} mouse line (Goebbels et al., 2006), which also induces recombination in dorsal telencephalic progenitors but specifically in intermediate progenitors in the subventricular zone and early postmitotic neurons, but not in RGC (Goebbels et al., 2006). Coronal slices of P1 mouse brains were stained with TAG1, a marker for corticofugal axons (green in Figures 1A–1F). TAG1 expression in NEX^{Cre};LKB1 cKO brains was indistinguishable from wild-type (WT) littermate brains (Figures 1A, 1B, 1D, and 1E), suggesting that axon specification is not impaired in NEX^{Cre};LKB1 cKO cortical neurons. In contrast, TAG1 immunoreactivity was entirely absent in Emx1^{Cre};LKB1 cKO brains, as reported previously (Figures 1C and 1F) (Barnes et al., 2007). Moreover, deletion of LKB1 in the NEX^{Cre} line did not recapitulate the high level of neuronal apoptosis observed in Emx1^{Cre};LKB1 cKO (Figures 1E and 1F) (Barnes et al., 2007), demonstrating that neuronal apoptosis in the Emx1^{Cre};LKB1 cKO is a direct consequence of not forming an axon rather than a consequence of not expressing LKB1.

In order to examine axon morphology at a single-cell resolution, we performed ex utero cortical electroporation at E15 of myristoylated-(m)Venus-expressing plasmid followed by dissociation of cKOs and littermates. After 5 days of culture in vitro (DIV), a significant fraction of Emx1^{Cre};LKB1 cKO neurons did not form an axon (defined by a neurite of length > 100 μm and positive for the axonal marker SMI312; Barnes et al., 2007; Shelly et al., 2007) (Figures S1A, S1B, and S1E available online). On the contrary, neuronal polarization was not affected in NEX^{Cre};LKB1 cKO neurons when compared to littermates (Figures S1C–S1E). Persistence of LKB1 expression in postmitotic neurons could not explain this result, as we observed that LKB1 expression was largely absent in NEX^{Cre};LKB1 cKO neurons cultures (Figure S1F). Taken together, our results indicate that LKB1 is required for axon specification in dividing progenitors during or shortly after cell cycle exit and that inactivating LKB1 in postmitotic neurons does not affect axon specification.

LKB1 Is Required for Axonal Branching In Vivo

NEX^{Cre};*LKB1*$^{F/F}$ mice were born viable and at Mendelian ratio. However, during the second postnatal week, the LKB1 cKO pups gained less weight than their littermates (Figure S1G) and, during the third postnatal week, showed an ~50% reduction in body weight even when solid or gelled food was made available in their cage bedding throughout weaning (Figure S1I). More than 70% of the LKB1 cKO pups ultimately died before P21 (Figure S1H), with P25 being the oldest NEX^{Cre};*LKB1*$^{F/F}$ cKO pup we could recover. We currently do not know why the mice die around weaning, but we discovered that NEX^{Cre} induces recombination in a subset of neurons from the peripheral nervous system innervating the intestine (J.C. and F.P., unpublished data), which might affect intestinal food absorption.

To circumvent this problem and in order to determine the cell-autonomous functions of LKB1 later during neuronal development in vivo, we performed in utero cortical electroporation (IUCE) at E15.5 of Cre-encoding plasmids in *LKB1*$^{F/F}$ mouse pups. This approach targets exclusively the progenitors of callosally projecting neurons in superficial layers 2/3 (Hand and Polleux, 2011; Mizuno et al., 2007; Wang et al., 2007). Electroporation was performed unilaterally in the somatosensory cortex, and axonal morphology of electroporated neurons was determined by expression of myristoylated (m)-Venus, which allowed (1) the cell-autonomous conditional ablation of LKB1 in callosally projecting neurons and (2) quantitative assessment of axon branching (Figures 1G–1Q). As shown previously (Hand and Polleux, 2011; Mizuno et al., 2007; Wang et al., 2007) (Figure S2), callosal axons cross the cortical midline, forming the corpus callosum (CC) around birth, and then reach the contralateral cortex during the first postnatal week and branch extensively between P8 and P21 in layers 2/3 and layer 5 while avoiding branching in layers 4 and 6 both ipsilaterally (Figures 1J and 1P) and contralaterally (Figures 1M and 1Q). We performed IUCE with a plasmid driving Cre-recombinase expression under a CMV early enhancer/chicken β-actin promoter (CAG::Cre) to induce robust recombination (Hand et al., 2005). Mice were sacrificed at P21 when callosal axons showed adult-like patterns of branching (Mizuno et al., 2007; Wang et al., 2007). LKB1-deficient axons formed, grew, and successfully crossed the midline (Figure 1H) but showed significantly reduced branching ipsilaterally in layer 5 (Figures 1K and 1P) and contralaterally both in layer 2/3 and 5 (Figures 1N and 1Q). We also used an independent Cre driver that drives recombination in postmitotic neurons (*Doublecortin*, DCX::Cre; Franco et al., 2011). Using this Cre driver, we observed a similar reduction in callosal axon branching both ipsilaterally and contralaterally (Figures 1I–1Q).

These effects on axon branching upon postmitotic deletion of LKB1 at P21 in vivo do not result from delayed axon development or axon degeneration because, in both control and Cre-electroporated brains, axons crossed the midline by P4 (Figures S2A, S2D, S2M, and S2N) and reached the contralateral side by P8 (Figures S2B, S2E, and S2O–S2Q). However, between P8 and P12, callosal axons from LKB1-deficient neurons failed to form discrete cortical columns contralaterally (Figures S2E,

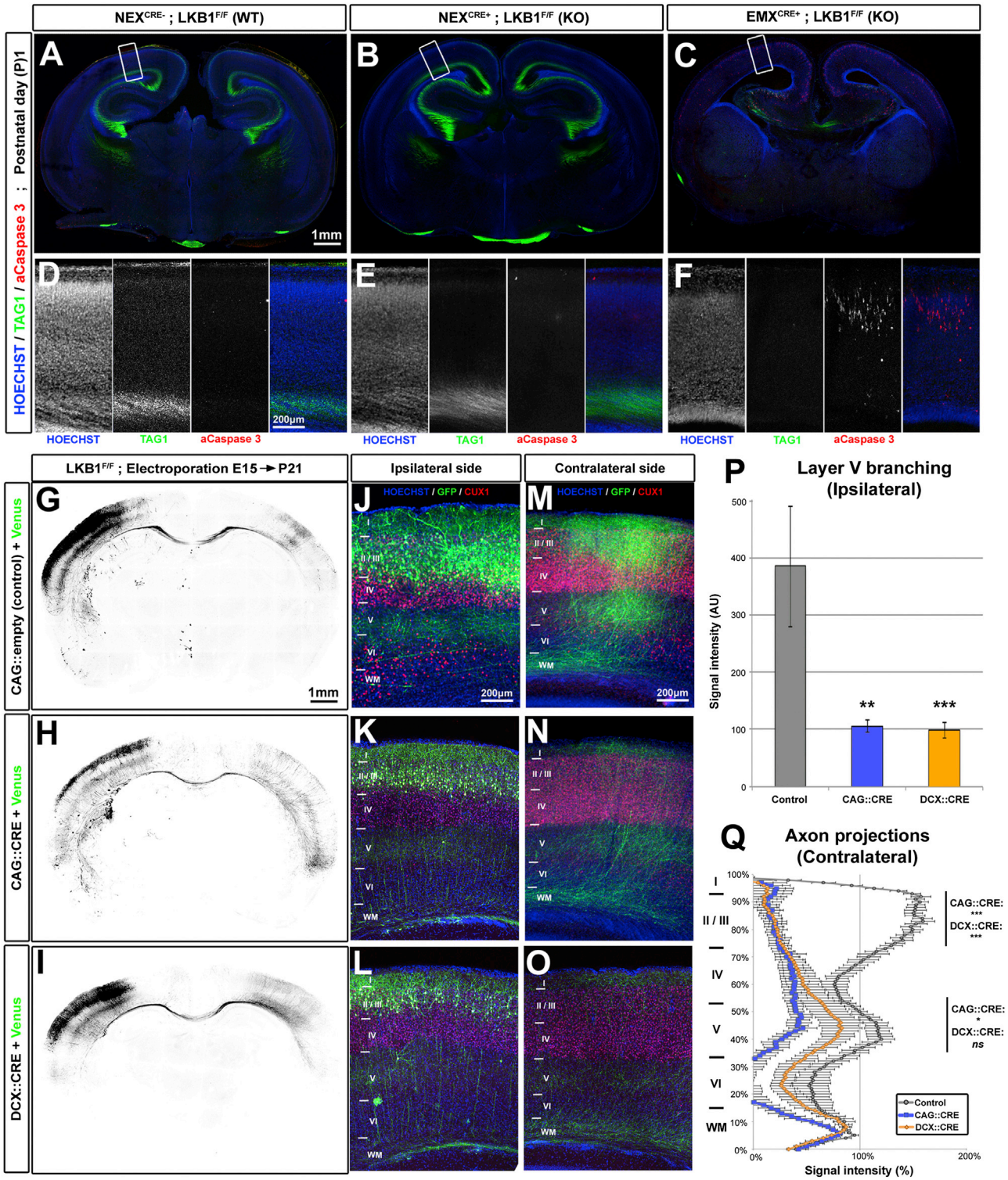

Figure 1. LKB1 Deletion after Axon Initiation Does Not Impair Axon Maintenance but Reduces Axon Branching In Vivo

(A–C) Coronal section of newborn *LKB1*$^{F/F}$ mouse brains not expressing Cre recombinase (WT) (A) or expressing Cre under the NEX (KO) (B) or EMX (KO) (C) promoters.

(D–F) Higher-magnification images of the cortex region boxed in (A), (B), and (C), respectively.

(G–I) Low-magnification images of coronal brain sections of P21 *Lkb1*$^{F/F}$ mice electroporated at E15 with plasmids expressing mVenus alone (G) or coexpressing Cre recombinase (under CAG promoter, H, or *Doublecortin* promoter, I) and mVenus.

(legend continued on next page)

S2F, and S2R) as seen in control (red arrowhead in Figures S2B, S2C, and S2P) and failed to branch (Figures S2C, S2F, and S2P–S2R), suggesting that LKB1-deficient neurons fail to induce terminal axon branching. The same lack of progressive branching in LKB1-deficient axons compared to control was observed ipsilaterally (Figures S2G–S2L). Overall, these results uncover a function for LKB1 in the control of axon branching in vivo.

NUAK1 Kinase Is Required for Axon Branching In Vivo

In order to identify which downstream kinase is the effector of LKB1 in mediating axon branching, we focused on two poorly studied AMPK-related kinases: NUAK1 and NUAK2. A previous report indicated that NUAK1 is highly expressed in the cortex during embryonic and postnatal development (Hirano et al., 2006), although its function during brain development is currently unknown. In situ hybridization on E14.5 WT mice revealed that both *Nuak1* and *2* are expressed in the embryonic brain (Figures 2A and 2B). *Nuak1* was expressed almost exclusively in the dorsal telencephalon and was restricted to the cortical plate (CP) containing postmitotic neurons (Figures 2A and 2A′). *Nuak2* expression was weaker and mostly restricted to the proliferative ventricular zone (VZ) of the cortex (Figures 2B and 2B′). We then compared NUAK1 and NUAK2 gene and protein expression in the cortex by RT-PCR and by western-blot at various pre- and postnatal ages (Figures 2C–2E). NUAK1 was expressed at all ages tested, although its expression decreased slightly at early postnatal stages but increased between P18 and adulthood in the cortex. On the contrary, *Nuak2* transcript was detected weakly and only in embryonic stages, and NUAK2 protein could not be detected at those ages. Quantitative RT-PCR indicated that *Nuak2* transcripts are 20 times less abundant than *Nuak1* transcripts at E15.5 (Figure 2E).

To confirm that NUAK1 is a relevant target of LKB1, we coexpressed both kinases in HeLa cells that are deficient for LKB1 expression. We observed that NUAK1 protein expression was increased when coexpressed with WT, but not with kinase-dead LKB1 (Figure 2F), as reported previously (Zagórska et al., 2010), suggesting that LKB1-mediated phosphorylation stabilizes NUAK1 protein. In agreement with this, we observed that NUAK1 protein expression was decreased in NEX^{Cre};LKB1 cKO neurons by nearly 50% compared of the control condition (Figure 2G). In order to confirm that NUAK1 catalytic activity is reduced in LKB1 cKO cortical neurons, we performed pull-down of endogenously expressed NUAK1 from cortical neurons in culture and assayed its ability to phosphorylate a NUAK1 target peptide (Figure 2H). We found a significant reduction in NUAK1 catalytic activity in the NEX^{Cre};$LKB1^{F/F}$ cKO neurons compared to both WT and heterozygous (HET) cortical neurons (Figure 2I). Because *Nuak1* appeared to be dominant over *Nuak2*, we selected short hairpin RNAs (shRNAs) against mouse *Nuak1* (Figures S3A and S3B) and used them to perform IUCE at E15.5. When mice were sacrificed at P21, we observed a significant reduction of callosal axon branching upon knockdown of *Nuak1* compared to control condition (Figures 2J and 2K, quantified in 2L) and to the same extent as LKB1 loss of function (Figures 1G–1Q). Taken together, these results indicate that NUAK1 kinase is required cell autonomously for cortical axon branching in vivo.

LKB1 and NUAK1 Kinases Are Required for Axon Branching In Vitro

In order to quantify axon morphology at a single-cell resolution, we examined the effects of *Lkb1* and *Nuak1* inactivation in vitro in dissociated neuronal cultures. We performed shRNA-mediated knockdown of *Lkb1* (Figure S3C) and *Nuak1* kinases or both *Nuak1* and *Nuak2* kinases using EUCE at E15.5 and observed that shRNA-electroporated neurons displayed significantly shorter and less-branched axons after 5 DIV (Figures 3B and 3C) compared to control shRNA (Figure 3A). Quantifications confirmed that *Lkb1* or *Nuak1* knockdown significantly reduced the length of the axon (Figure 3G) and also significantly reduced overall axon branching compared to control electroporation (Figure 3H). Knocking down *Nuak2*, together with *Nuak1*, did not show any additive effects compared to *Nuak1* alone, suggesting that these two kinases are not redundant with regard to axon growth and branching.

We independently examined the consequences of complete genetic loss of *Lkb1* or *Nuak1* by electroporation of a Venus-encoding plasmid in $NUAK1^{-/-}$ neurons (Figures S3D and S3E; Hirano et al., 2006) and of CAG::CRE or DCX::CRE plasmids in $LKB1^{F/F}$ neurons (Figures S3G–S3I). Quantifications confirmed that axon length and axon branching are significantly reduced in LKB1 or NUAK1 null cortical neurons when compared to the control (Figures S3F, S3J, and S3K). These effects seemed largely specific to the axon because neither deleting *Lkb1* nor knocking down *Nuak1* had a significant effect on the number of primary MAP2+ dendrites emerging from the cell body (Figure S3M) and that *Nuak1* knockdown did not affect dendritic length at 5 DIV.

LKB1 and NUAK1 Regulate Both Axon Growth and Branching Independently of Axon Specification

We tested whether the decrease in axon branching could be a secondary consequence of impaired axon growth. Axon branching was still decreased in both LKB1 and NUAK1 loss-of-function experiments even when axon branch number was normalized for axon length (Figures 3I and S3L). To better visualize the dynamics of axon growth and branching, we performed long-term (15 hr) time-lapse imaging of neurons lacking *Lkb1* or *Nuak1* (Figured S4A–S4F and Movie S1). We observed that the axon growth rate was decreased upon loss of either *Lkb1* or *Nuak1* (Figure S4G). Importantly, we also observed that loss of function of either *Lkb1* or *Nuak1* impaired axon branch initiation (for both *Lkb1* and *Nuak1* loss of function) and branch stability

(J–O) Higher magnification of the ipsilateral (J–L) or the contralateral side (M–O) showing reduced axon branching in both Cre-electroporated neurons (K–O) compared to control (J and M).

(P–Q) Quantification of normalized Venus fluorescence in layer 5 of the ipsilateral cortex (P, ± SEM) and along the radial axis of the cortical wall in the contralateral cortex (Q, ± SEM). Statistical analysis: Mann-Whitney (P) or two-way analysis of variance (ANOVA) (Q).

See also Figures S1 and S2.

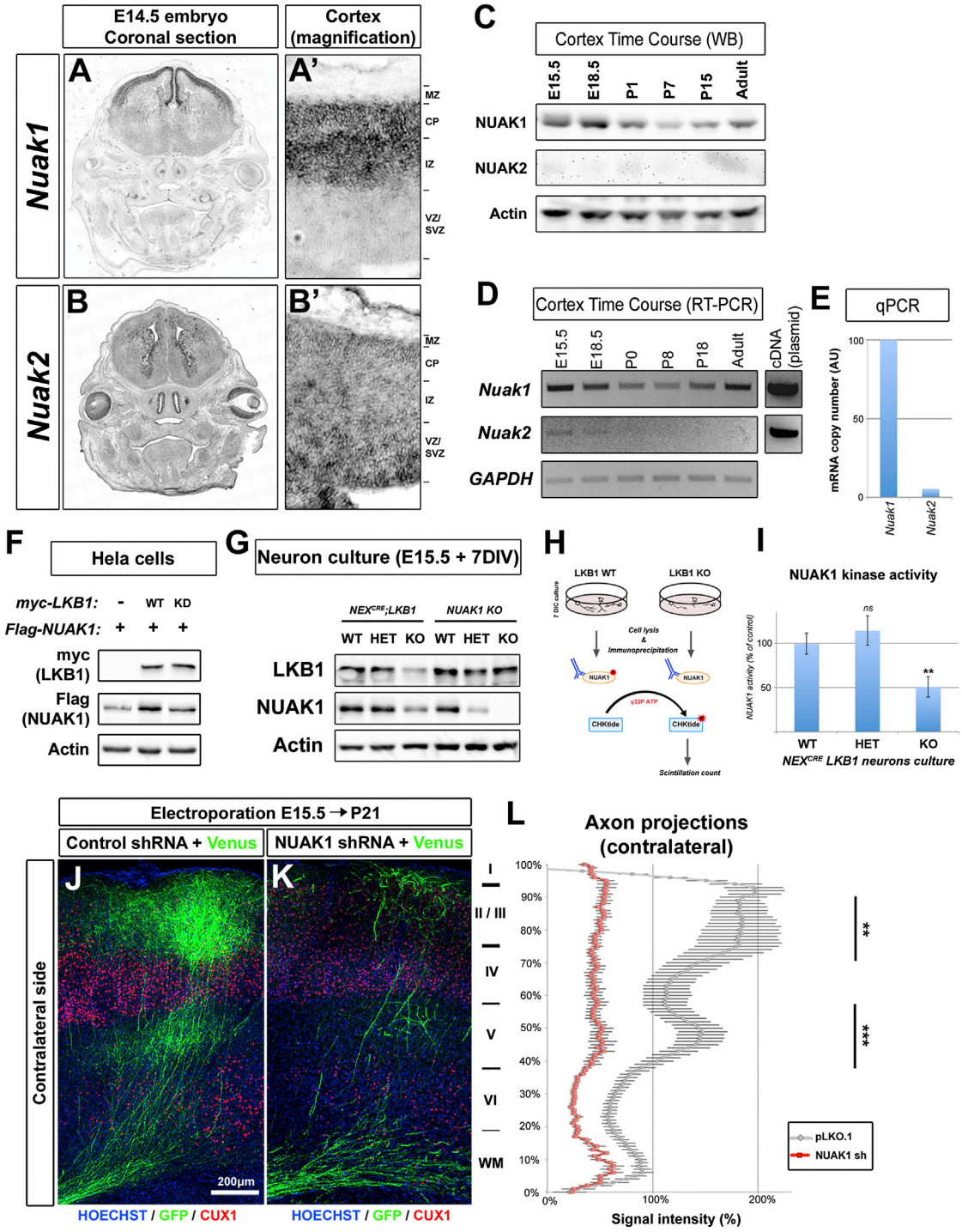

Figure 2. AMPK-Related Kinase NUAK1 Is Required for Axon Branching In Vivo

(A and B) Expression of *Nuak1* and *Nuak2* genes in the head of Balb/C mouse by in situ hybridization. Magnification (A′–B′) shows that *Nuak1* and *Nuak2* have complementary expression patterns in the cerebral cortex.

(C) Time course of NUAK1 and NUAK2 protein expression in Balb/C mouse cortex by western blot.

(D) Time course of *Nuak1* and *Nuak2* mRNA expression in Balb/C mouse cortex by RT and PCR.

(E) Quantitative PCR after RT (qRT-PCR) in E15.5 mouse cortex revealed that the *Nuak1* transcript is 20 times more abundant than the *Nuak2* transcript.

(F) Overexpression of catalytically active LKB1 increases NUAK1 protein expression.

(G) Endogenous expression of LKB1 and NUAK1 proteins in LKB1 and NUAK1 knockout neurons. Western blot analysis was performed with the indicated antibodies.

(legend continued on next page)

(for *Lkb1* loss of function) (Figure S4H), thus demonstrating that LKB1 and NUAK1 regulate both axon growth and axon branching.

In accordance to previous results (Barnes et al., 2007; Shelly et al., 2007) and as shown in Figures S3H and S3I, both CAG::Cre- and DCX::Cre-mediated *Lkb1* deletion results in a small but significant percentage of cortical neurons that do not form an axon under these conditions (~40% with CAG::Cre and 19% with Dcx::Cre compared to 11% in control neurons). However, this is in stark contrast with genomic recombination using $Emx1^{Cre}$, which, in the same culture conditions, leads to more than 80% of cortical neurons without an axon (Figures S1B and S1E). Thus, we wanted to test unequivocally whether the effect of LKB1 on axon growth and branching was indirectly linked to their effects on axon specification through a delay in axon formation. To test this, we performed Cre transfection in $LKB1^{F/F}$ cortical cultures (Figures S3N and S3O) at 3 DIV (i.e., after axon polarization and during the main phase of axon growth) (Barnes et al., 2007). Our results demonstrate that, at 7 DIV, LKB1-deficient neurons show a decrease in axon branching (but no decrease in axon growth) compared to control (Figures S3P and S3Q). Collectively, these results demonstrate that LKB1 controls both axon growth and branching but that one can operationally segregate the effects on axon branching from the effect on the main axon growth.

NUAK1 Is Required Downstream of LKB1 for Axon Growth and Branching

We tested whether overexpression of LKB1 or NUAK1 was sufficient to promote axon growth and/or axon branching. After 5 DIV, we observed that overexpression of LKB1 or NUAK1 was sufficient to induce a marked increase in axon branching (Figures 3D–3F and 3K) without a significant effect on axon length (Figure 3J) compared to control.

We then took advantage of this overexpression-mediated increase in axon branching and tested functional epistasis between LKB1 and NUAK1. We found that knockdown of *Nuak1* suppressed the increase in axon branch number induced by LKB1 overexpression (Figures 3J and 3K), suggesting that NUAK1 is the main downstream effector of LKB1 during axon growth and branching. Moreover, overexpression of NUAK1 was sufficient to rescue *Lkb1* loss of function (Figures 3J and 3K), whereas simultaneous knockdown of *Lkb1* and *Nuak1* showed no additive decrease in axon length or axon branch number (Figures 3G–3I), indicating that LKB1 and NUAK1 form a kinase pathway controlling axon growth and branching.

To further explore the specificity of NUAK1 in axon branching, we tested the consequences of overexpressing other LKB1-dependent AMPK-like kinases on axon branching. None of the other members of the AMPK-like kinase family we tested, including NUAK2, SAD-B, and AMPKα2, had any significant effect on axon growth or branching by overexpression (Figures S5A–S5F), despite comparable levels of overexpression (Figure S5G). As SAD-A/B have been previously shown to regulate polarity in cortical neurons (Barnes et al., 2007; Kishi et al., 2005), we tested whether they were required for cortical axon growth or branching in vitro. shRNA-mediated knockdown of *Sad-A/B* (Figures S5L and S5M) had no effect on cortical axon growth or branching at 5 DIV in the fraction of neurons that successfully formed an axon (Figures S5H–S5K).

Loss of LKB1 or NUAK1 Increases Mitochondrial Motility in the Axon

How do LKB1-NUAK1 kinases control axon growth and branching? MARK1–4 kinases are downstream effectors of LKB1 in some cell types and have been shown to regulate microtubule dynamics (Mian et al., 2012; Nishimura et al., 2012). Furthermore, axon growth and branching is dependent on microtubule dynamics (Gallo, 2011; Polleux and Snider, 2010). We therefore tested whether LKB1 or NUAK1 affected microtubule stability and/or dynamics in developing axons. First, we found no difference in the ratio of tyrosinated and acetylated tubulin (Figure S6H), an index of stable versus dynamic microtubules, in *Lkb1*- or *Nuak1*-deficient neurons. To explore effects on microtubule dynamics specifically in the growing axon, we used EB3-EGFP (a marker of the polymerizing end of microtubules) in control or *Nuak1* shRNA electroporated neurons and then performed time-lapse imaging of EB3-EGFP "comets" in axonal growth cones at 5 DIV (Figures S6I–S6L and Movie S2). We observed no significant difference in the total area of the growth cone explored by microtubules (Figure S6M), EB3-comets velocity (Figure S6N), or lifetime (Figure S6O), suggesting that the effects of LKB1-NUAK1 kinases on axon growth and branching are unlikely to be due to changes in microtubule dynamics.

Axonal transport and targeting of presynaptic cargoes to nascent presynaptic sites has been previously implicated in both axonal growth and branch stabilization, especially during activity-dependent phases of synaptic formation (Meyer and Smith, 2006; Ruthazer et al., 2006; Takeda et al., 2000). Therefore, we tested whether axonal transport was defective in LKB1- and NUAK1-deficient cortical neurons using fluorescently labeled organelles or presynaptic vesicles coupled to time-lapse microscopy in axons. LKB1 null cortical neurons at 7 DIV did not show any defect in the axonal transport of synaptic vesicle precursors labeled with VGLUT1-Venus (Herzog et al., 2011) (Figures S6A–S6D and Movie S2). On the other hand, we observed a striking change in mitochondrial axonal transport visualized using time-lapse microscopy of 5 DIV cortical neurons expressing mitoDsRed (Figures 4A and 4B and Movie S3). As reported previously, in WT growing hippocampal or cortical axons, mitochondria have a characteristic motility profile in which ~65% of the mitochondrial pool is stationary, whereas

(H) Schema of NUAK1 kinase assay.

(I) NUAK1 kinase activity is reduced in LKB1 KO neurons (± SEM).

(J and K) In utero cortical electroporation of the indicated constructs revealed that loss of NUAK1 decreased axonal branching in the contralateral hemisphere similar to the loss of LKB1.

(L) Quantification of EGFP normalized fluorescence along the radial axis of the cortical wall in the contralateral cortex. Statistical analysis: Mann-Whitney test (I) or two-way ANOVA (L) (± SEM).

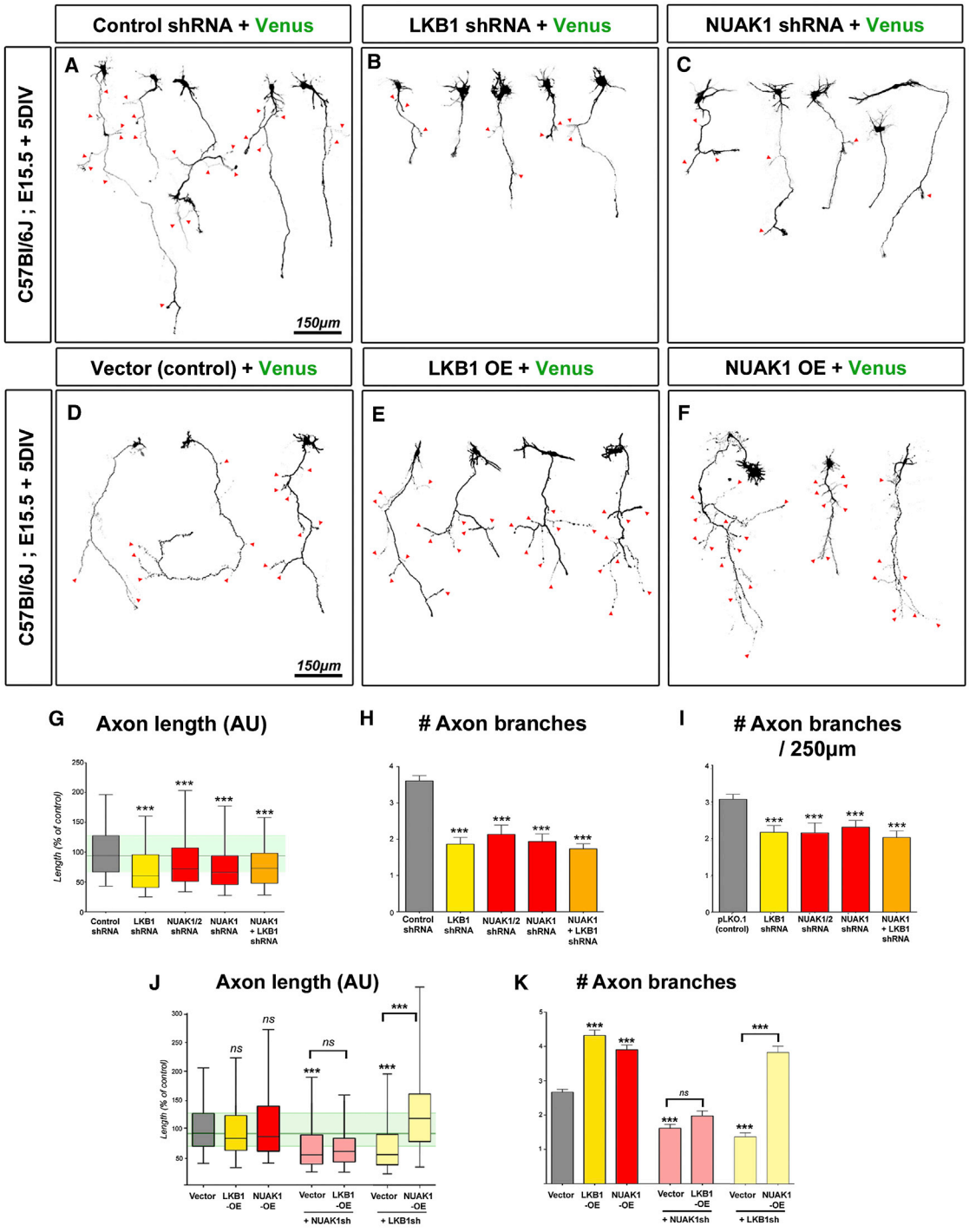

Figure 3. LKB1 Regulates Axon Growth and Branching In Vitro through NUAK1

(A–C) Representative neurons imaged after 5 DIV following inhibition of LKB1 (B) or NUAK1 (C) expression.

(D–F) Overexpression of LKB1 (E) or NUAK1 (F) in 5 DIV cortical neurons induced the formation of supernumerary axonal branches. Red arrowheads in (A)–(F) point to axon branches.

(G–I) Quantification of axon morphology shows that LKB1 or NUAK1 inhibition results in a shortened axon (G) and decreased collateral branch formation (H and I).

(J and K) Quantitation of axon length (J) or number of collateral branches at 5 DIV (K) after overexpression of the indicated constructs. Data represent 25th, 50th, and 75th percentile (G and J) or average value ± SEM (H, I, and K). Statistical analysis: Mann-Whitney test.

See also Figures S3, S4, and S5.

the other 35% are transported in both the anterograde and retrograde directions (for example, see Brickley and Stephenson, 2011; Wang et al., 2011). Upon loss of LKB1, we observed a 3-fold decrease in the percentage of immobilized mitochondria along the axon shaft (Figures 4A, 4B, and 4G and Movie S3). Importantly, a similar phenotype was observed in *Nuak1* KO cortical neurons (Figures 4C, 4D, and 4G and Movie S3). Motile mitochondria in the axon of *Lkb1* and *Nuak1* null cortical neurons also displayed increased maximum instantaneous velocity as well as increased maximum distance traveled, both anterogradely and retrogradely, compared to controls (Figures S6E and S6F). These changes in motility were not accompanied by detectable changes on mitochondria density along the axon shaft (Figure S6G). Conversely, overexpression of either LKB1 or NUAK1 was sufficient to increase significantly (from ~60% to 75%) the proportion of stationary mitochondria along the axon (Figures 4E, 4F, 4H, and 4I). Accordingly, dwell time of motile mitochondria also decreased upon loss of LKB1 or NUAK1 (Figures 4J and 4L) and increased with the overexpression of either LKB1 or NUAK1 (Figures 4K and 4L).

Syntaphilin Is Required for Proper Callosal Axon Branching In Vitro and In Vivo

We next wanted to test whether there was a causal relationship between axon branching and the ability of mitochondria to become immobilized along the axon. To accomplish this, we needed a tool that would allow us to specifically regulate mitochondria immobilization along the axon. Syntaphilin (SNPH) is an axonally targeted, mitochondria-associated protein that also binds microtubules (Kang et al., 2008). Importantly, cortical neurons isolated from *Snph* knockout mice showed decreased mitochondria immobilization (Kang et al., 2008), a phenotype that is qualitatively and quantitatively very similar to *Lkb1* and *Nuak1* null cortical neurons. We first tested whether the loss of SNPH affected axonal branching by using electroporation of shRNA against mouse *Snph* (Figure 5A) in cortical progenitors at E15.5 by EUCE. We confirmed that knockdown of mouse *Snph* significantly decreased the percentage of immobile mitochondria in cortical axons (Figures 5B, 5C, and 5J and Movie S4) to a level comparable to that observed in *Snph* null neurons (Kang et al., 2008) and *Lkb1* or *Nuak1* null neurons. Interestingly, knockdown of *Snph* significantly decreased axon branching in cortical neurons in vitro (Figures 5F, 5G, and 5K). These results are phenocopied by the overexpression of a dominant-negative SNPH that is targeted to the axon and can bind mitochondria but lacks its microtubule-binding domain (SNPH-ΔMTB) (Kang et al., 2008) (Figures 5E and 5I–5K and Movie S4). Furthermore, overexpression of SNPH, which significantly increased the percentage of stationary mitochondria along cortical axons (Figures 5D and 5J and Movie S4), was sufficient to increase axon branching at 5 DIV (Figures 5H and 5K). Finally, IUCE of shRNA against *Snph* revealed that SNPH in vivo is required for terminal axon branching on both the ipsilateral and contralateral hemispheres in layers 2/3 and 5 (Figures 5O–5Q) when compared to control (Figures 5L–5N). Upon quantification, the reduction of axon branching upon shRNA electroporation was of similar magnitude to the reduction observed upon loss of LKB1 both ipsilaterally (Figure 5R) and contralaterally (Figure 5S). These results establish that SNPH is required for proper axon branching both in vitro and in vivo and suggests that there is a direct link between mitochondria immobilization and axon branching.

LKB1 Regulates Axon Branching by Controlling Mitochondrial Immobilization

We took advantage of the fact that overexpression of full-length SNPH is sufficient to arrest mitochondria motility (Kang et al., 2008; Figure 5D) to determine whether there was a causal relationship between mitochondria immobilization and LKB1-dependent axonal branching. We confirmed the decrease in the percentage of stationary mitochondria (Figures 6A, 6B, and 6K) and the decreased axon branching in LKB1-deficient neurons compared to control neurons at 5 DIV (Figures 6F, 6G, and 6L). Remarkably, SNPH overexpression to levels that restored the percentage of immobile mitochondria back to control levels in *Lkb1* null neurons (Figures 6C and 6K and Movie S5) also rescued axonal branching to control levels (Figures 6H and 6L).

As shown previously, we confirmed that LKB1 overexpression increased both axonal branching and the percentage of stationary mitochondria in the same neuronal cultures when compared to control neurons (Figures 6D, 6I, 6M, and 6N and Movie S5). Expressing SNPH-ΔMTB in LKB1-overexpressing cortical neurons restored the percentage of stationary mitochondria to ~60% (Figures 6E and 6M) and rescued axonal branching to levels comparable to control (Figures 6J and 6N). These results demonstrate that LKB1 controls axonal branching by regulating mitochondria immobilization.

LKB1 and NUAK1 Induce Mitochondria Immobilization at Nascent Presynaptic Sites along the Axon

Based on previously published work demonstrating that presynaptic transport and synapse formation positively regulate axon branch stabilization (Meyer and Smith, 2006; Ruthazer et al., 2006) and that mitochondria are highly enriched at presynaptic sites in many axon types (Harris and Weinberg, 2012), we tested whether LKB1 and NUAK1 were specifically regulating mitochondrial immobilization and/or long-term capture at nascent presynaptic sites. We performed dual-channel time-lapse imaging at 7 DIV in cortical axons of dissociated neurons electroporated with VGLUT1-Venus and mito-DsRed by EUCE at E15.5. The vast majority of VGLUT1-Venus puncta overlap with two other presynaptic vesicle proteins (Synaptobrevin 2 and Synapsin1) or the presynaptic active zone scaffolding protein Bassoon (Figure S7; Sabo et al., 2006), confirming that VGLUT1-Venus faithfully detects nascent presynaptic sites along developing cortical axons (Herzog et al., 2011).

We determined that LKB1 or NUAK1 downregulation or overexpression do not affect the density of stable (defined as stationary for 30 min of time-lapse) VGLUT1-Venus puncta (Figures 7A, 7C, and 7E; quantified in Figures 7G and 7J and Movie S6). Using dual time-lapse microscopy of VGLUT1-Venus and mito-DsRed in WT axons, we observed that many motile mitochondria frequently dwelled over stable VGLUT1-Venus puncta, often before resuming movement (Figures 7A and 7B and Movie S6). However, in LKB1- and NUAK1-deficient axons, we observed a significant decrease in the colocalization of

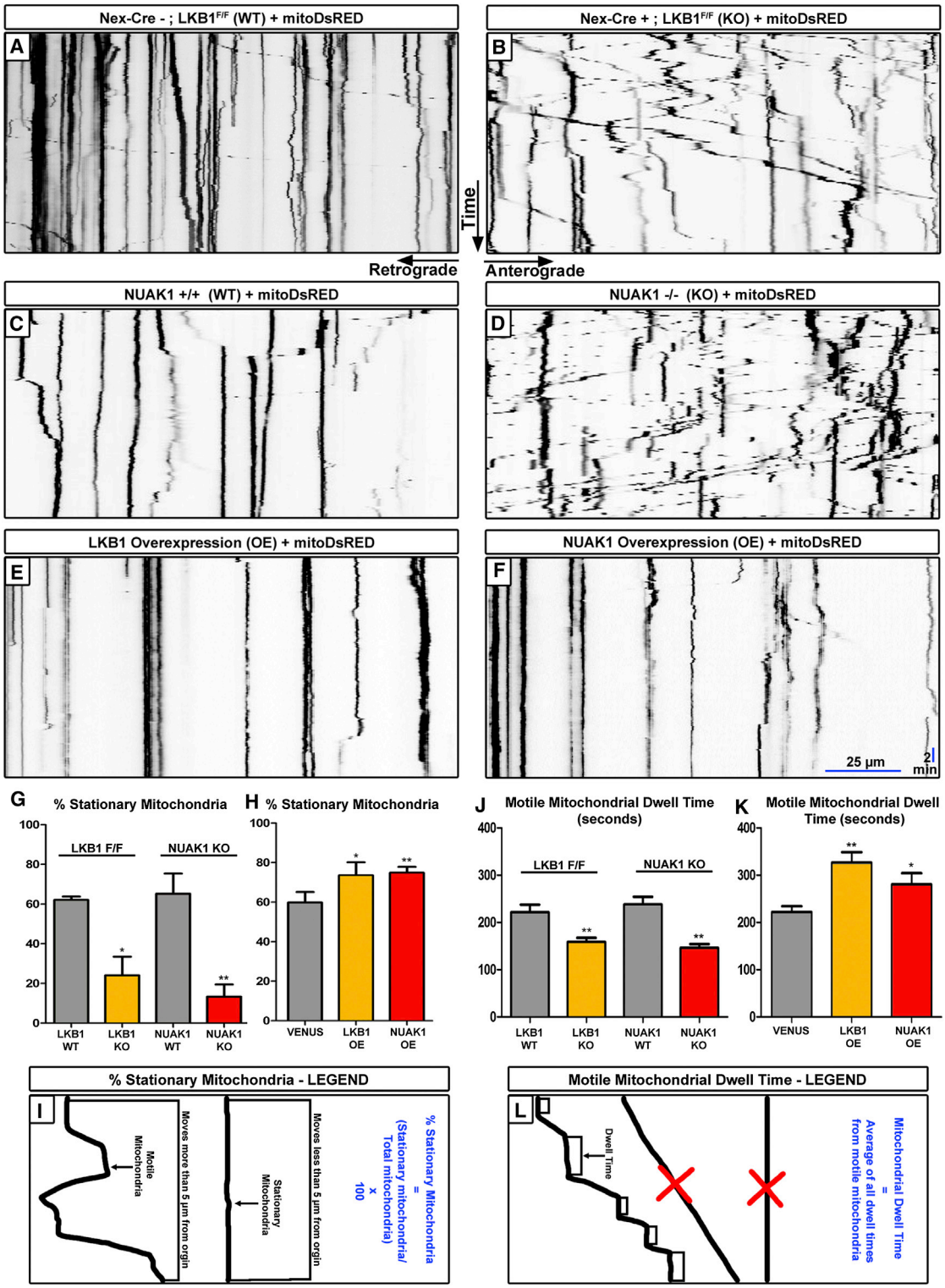

Figure 4. LKB1 and NUAK1 Are Necessary and Sufficient for Mitochondrial Immobilization in Cortical Axons

(A–F) Representative kymographs of axonal mitochondria in dissociated neurons electroporated with the indicated constructs.

(G and H) (G) Loss of LKB1 or NUAK1 caused a significant decrease in the number of stationary mitochondria, (H) whereas overexpression of LKB1 or NUAK1 produced more stationary mitochondria (±SEM).

(J and K) (J) Loss of LKB1 or NUAK1 led to a decrease in motile mitochondrial dwell time, (K) whereas overexpression of LKB1 or NUAK1 increased the dwell time of motile mitochondria (±SEM).

(legend continued on next page)

motile mitochondria over stable VGLUT1 puncta (Figures 7C and 7D). Strikingly, the loss of LKB1 or NUAK1 led to a 50% reduction in the average time that motile mitochondria spent dwelling over nascent presynaptic sites but, importantly, did not affect the average dwelling time outside presynaptic boutons (Figures 7G–7I). LKB1 or NUAK1 are also sufficient to instruct mitochondria to specifically dwell at nascent presynaptic sites (Figures 7G–7I).

Finally, we found that loss of LKB1 or NUAK1 significantly reduced mitochondria long-term capture (immobilized for 30 min as opposed to transient dwelling; Figure 7G) presynaptically by more than 50%, whereas overexpression of LKB1 or NUAK1 increased by more than 2-fold the percentage of stationary mitochondria captured presynaptically (Figure 7K). These results demonstrate that LKB1 and NUAK1 kinases are specifically involved in immobilization (dwelling or capture) of mitochondria at nascent presynaptic sites.

DISCUSSION

The polarization of cortical neurons is tightly coupled to neuron migration, during which immature neurons form two molecularly and functionally distinct compartments (Barnes and Polleux, 2009): the somato-dendritic domain and the axon. LKB1 is necessary and sufficient for axon specification in vitro and in vivo (Barnes et al., 2007; Shelly et al., 2007). Our present results demonstrate that LKB1 is required in newly born neurons at the time of cell cycle exit or shortly thereafter to instruct neuron polarization.

We demonstrate here—using various in vitro and in vivo strategies—that LKB1 is necessary and sufficient for terminal axon branching of cortical neurons through the activation of NUAK1, an AMPK-related kinase whose function during brain development was unknown. NUAK1 seems to be the main effector of LKB1 in mediating axon growth and branching in cortical neurons. Our results do not exclude that other AMPK-related kinases might have a less prominent or redundant role during axon growth and branching. We observed that NUAK1 expression is largely restricted in the dorsal telencephalon in the embryo, as previously reported (Hirano et al., 2006). Whether LKB1 is required for axon growth or branching in other types of neurons and whether this function involves NUAK1 or other AMPK-related kinases remain to be determined. The SAD kinases are required in cortical neurons to mediate LKB1-dependent polarization (Barnes et al., 2007; Kishi et al., 2005). Therefore, it appears that LKB1 controls at least two kinase pathways in cortical neurons during development: SAD-A/B for axon specification and NUAK1 for axon growth and branching. How SAD-A/B and NUAK1 kinases are differentially regulated by LKB1 during development is currently unknown. Interestingly, SAD-A/B kinases also play a role in presynaptic development and synaptic vesicle release (Crump et al., 2001; Inoue et al., 2006), suggesting that their function downstream of LKB1 extends beyond axon specification.

Mitochondria are critical to many functions in cells, including ATP production, calcium homeostasis, and the triggering of apoptosis through release of cytochrome-c (Schon and Przedborski, 2011; Sheng and Cai, 2012). The high-energy demand of neurons requires that mitochondria be readily available throughout the large cytoplasmic volume of neurons and, in particular, be trafficked properly along the entire length of the axon where presynaptic release consumes a large amount of ATP (Vos et al., 2010). Our results suggest that immobile mitochondria have a unique property with regard to their ability to stimulate axon branching not shared by mobile mitochondria through promotion of axon branch formation and/or branch stabilization. Further work is needed to determine the precise mechanisms by which LKB1 and NUAK1 regulate mitochondrial capture presynaptically, including the role of syntaphilin in this process. Currently, we have no evidence of direct interaction or phosphorylation of SNPH by either LKB1 or NUAK1 (J.C. and F.P., unpublished data); however, this does not exclude the involvement of other intermediate kinases or adaptor proteins regulating SNPH-mediated immobilization of mitochondria. Future investigations will determine how LKB1-NUAK1-regulates the capture of mitochondria to nascent presynaptic sites and how this capture regulates axon branching through control of ATP production and/or Ca^{2+} homeostasis or through other unknown mechanisms.

EXPERIMENTAL PROCEDURES

Animals

All animals were handled according to protocols approved by the Institutional Animal Care and Use Committee (IACUC) at University of North Carolina at Chapel Hill and at The Scripps Research Institute, La Jolla, CA. Timed-pregnant females were maintained in a 12 hr light/dark cycle and obtained by overnight breeding with males of the same strain. For timed-pregnant matings, noon after mating is considered embryonic day 0.5 (E0.5). Ex vivo cortical dissociation of neurons was performed on C57Bl/6J or on Balb/C timed-pregnant mice. Floxed LKB1 mice ($Stk11^{tm1.1Rdp}$) and $Emx1^{Cre}$ transgenic mice ($Emx1^{tm1(cre)Ito}$) have been used previously (Barnes et al., 2007). NEX^{Cre} mice ($NeuroD6^{tm1(cre)Kan}$) were obtained from the Jackson laboratory. NUAK1 KO mice ($Nuak1^{tm1Sia}$) were described previously (Hirano et al., 2006).

In Utero Cortical Electroporation

The previously described protocol for in utero cortical electroporation (Hand and Polleux, 2011) was modified as follows. Timed-pregnant hybrid F1 females were obtained by mating inbred 129/SvJ females, and C57Bl/6J males and were used for shRNA electroporation. Timed-pregnant $LKB1^{F/F}$ females were used for Cre plasmid electroporation. A mix of endotoxin-free plasmid preparation (Cre plasmid or shRNA plasmid mix ~1 μg/μl, except SNPH shRNA at 0.5 μg/μl and the reporter plasmid pSCV2 ~0.5 μg/μl) was injected into one lateral hemisphere of E15.5 embryos using a picospritzer. Electroporation was performed with gold paddles to target cortical progenitors in E15.5 embryos by placing the anode (positively charged electrode) on the side of DNA injection and the cathode on the other side of the head. Four pulses of 45 V for 50 ms with 500 ms interval were used for electroporation.

(I) Kymograph illustration of the parameters used to determine motile and stationary mitochondria.
(L) Schema illustrating the parameters used to determine mitochondrial dwell time. Motile mitochondria that did not pause for at least 60 s were excluded, as were stationary mitochondria. All kymographs throughout the paper are oriented as shown in (A) and (B). Statistical analysis: Mann-Whitney test.
See also Figure S6.

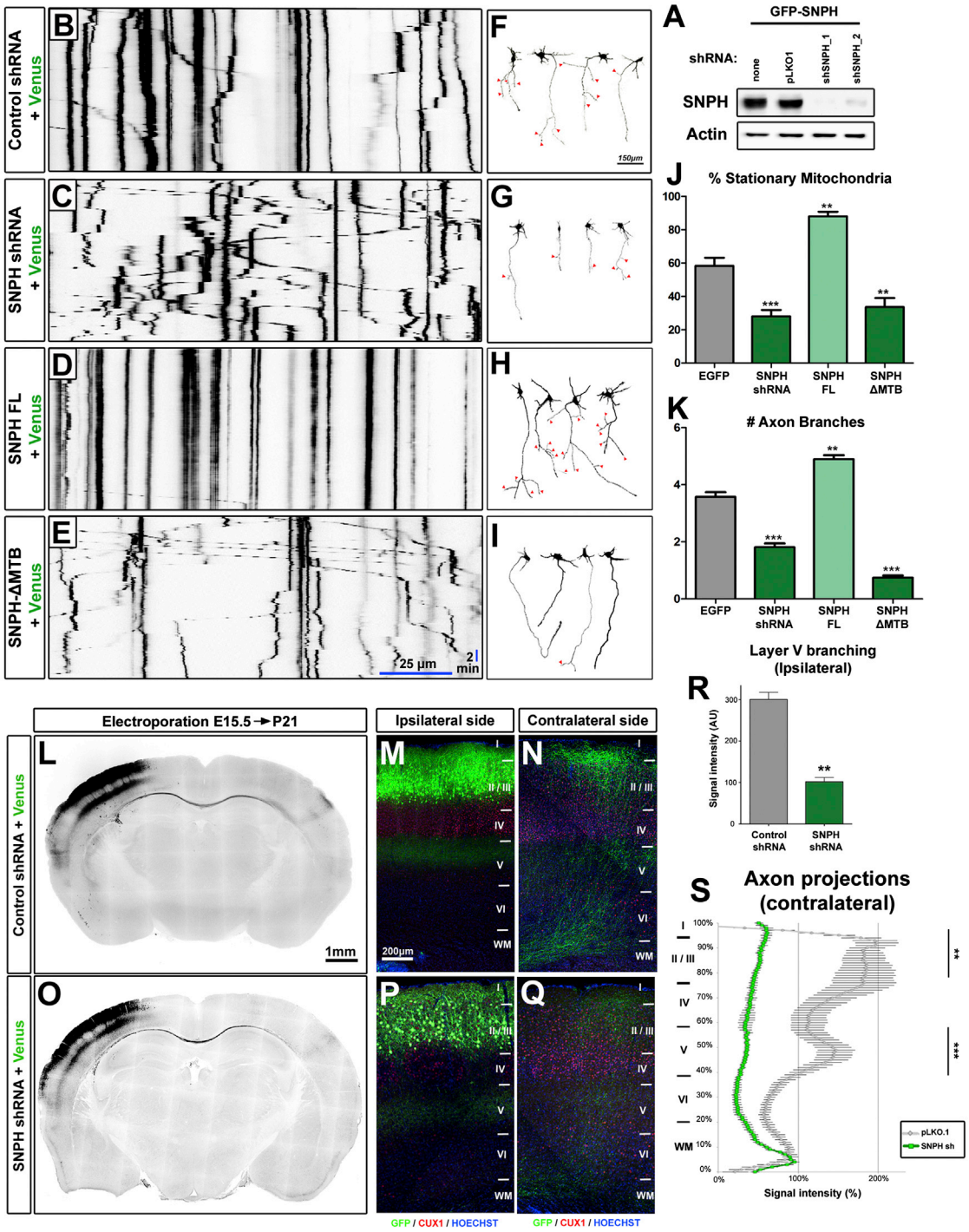

Figure 5. Syntaphilin-Dependent Mitochondria Immobilization Is Necessary and Sufficient for Proper Axon Branching

(A) Validation of shRNA targeting mouse *Snph* in HEK293T cells. Western blot analysis was performed with the indicated antibodies.

(B–E) Representative kymographs of axonal mitochondria in dissociated neurons electroporated with the indicated constructs.

(F–I) Representative neurons at 5 DIV electroporated with the constructs indicated in (B)–(E). Red arrowheads point to axon branches.

(J and K) Loss or disruption of SNPH decreased, whereas overexpression of SNPH increased the number of stationary mitochondria (J) and of axonal branches (K).

(L–Q) Low magnification images of coronal brain sections at P21 (L and O) and high magnification for the ipsilateral (M and P) or contralateral (N and Q) side.

(R) Loss of SNPH caused a reduction in axonal branching on layer 5 of the ipsilateral hemisphere.

(S) Loss of SNPH reduced axonal branching in both layers 2/3 and 5 of the contralateral hemisphere. Data represent average value ± SEM (J, K, R, and S). Statistical analysis: Mann-Whitney test or two-way ANOVA (S).

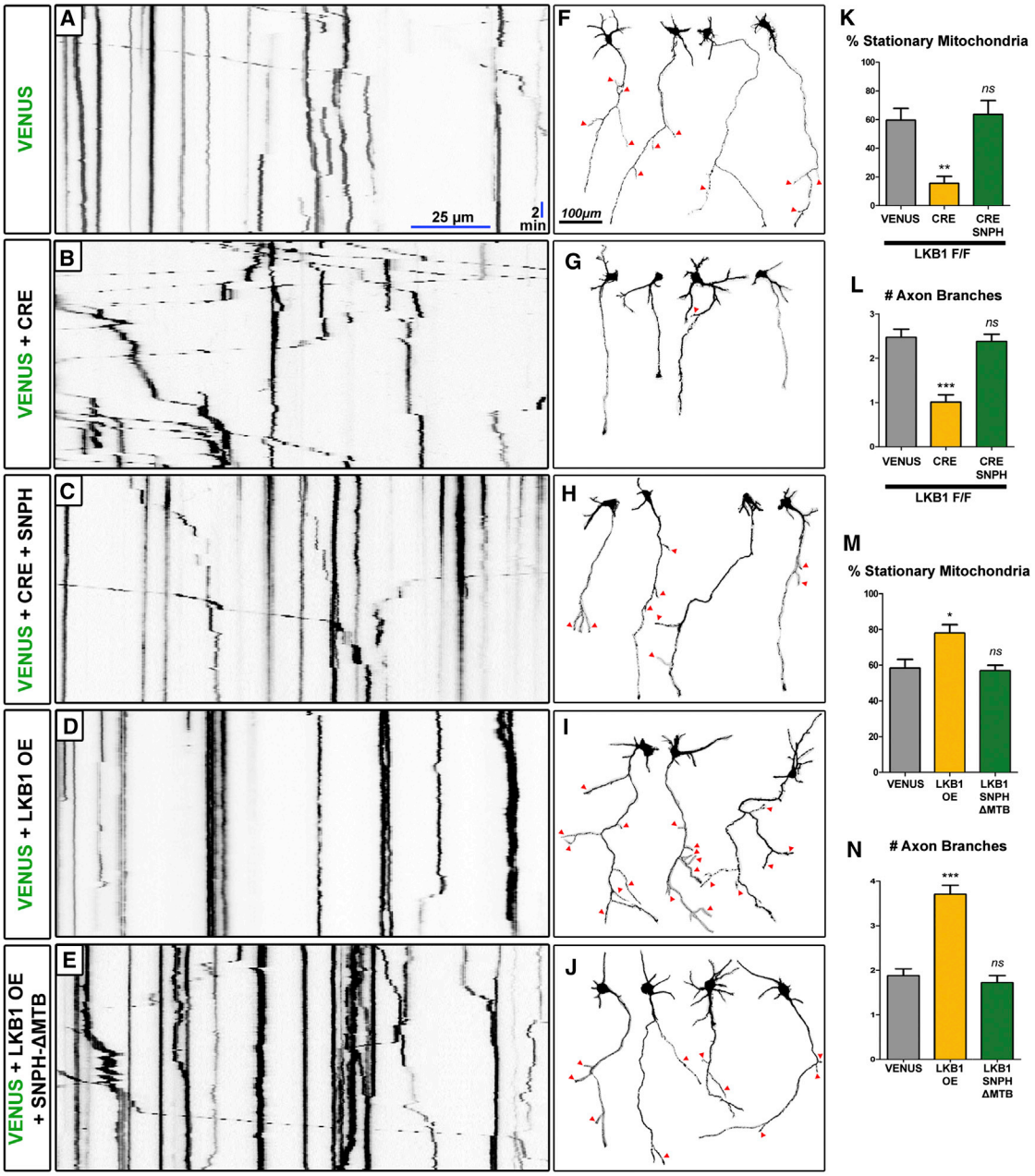

Figure 6. LKB1 Mediates Axonal Branching through Mitochondria Immobilization along the Axon

(A–E) Representative kymographs of axonal mitochondria in dissociated neurons electroporated with the indicated constructs.

(F–J) Representative neurons at 5 DIV electroporated with the constructs indicated in (A)–(E). Red arrowheads point to axon branches.

(K) Loss of LKB1 caused a decrease in the percentage of stationary mitochondria, whereas overexpression of WT human SNPH upon loss of LKB1 returned mitochondrial transport to normal levels.

(L) Loss of LKB1 decreased the number of axonal branches, whereas overexpression of WT human SNPH upon loss of LKB1 returned axonal branching to normal levels.

(M) Overexpression of LKB1 increased the percentage of stationary mitochondria, whereas overexpression of dominant-negative human SNPH-ΔMTB at the same time as LKB1 returned mitochondrial transport to normal levels.

(N) Overexpression of LKB1 also increased the number of axonal branches, whereas overexpression of dominant-negative human SNPH-ΔMTB at the same time as LKB1 returned axonal branch number to normal levels.

Data represent average value ± SEM (K–N). Statistical analysis: ANOVA nonparametric test.

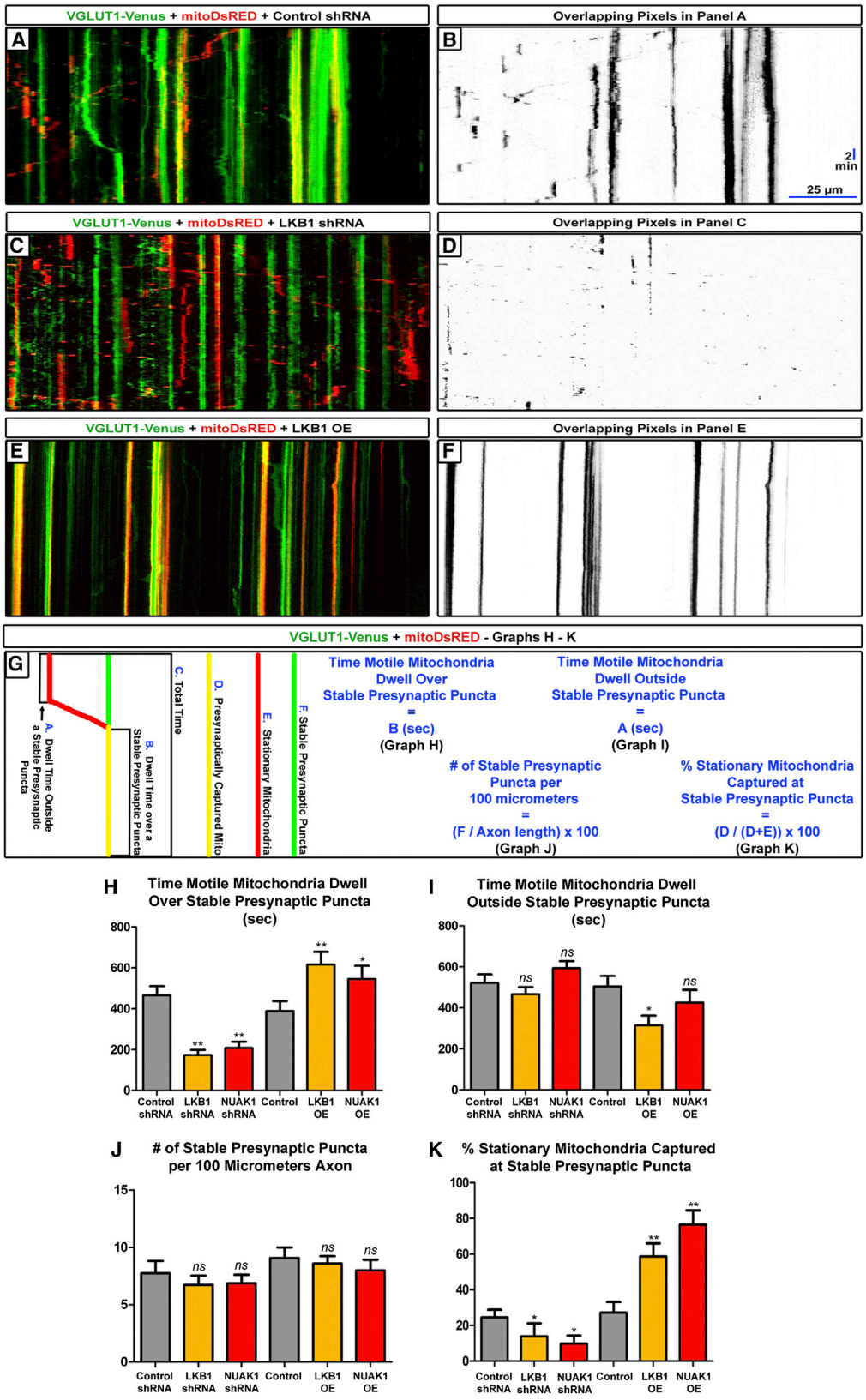

(legend on next page)

Animals were sacrificed 3 weeks after birth by terminal perfusion of 4% paraformaldehyde (PFA, Electron Microscopy Sciences) followed by 2 hr postfixation in 4% PFA.

Ex utero cortical electroporation, followed by dissociation and cortical neuron culture, was performed as previously described (Hand et al., 2005). See Supplemental Information for details.

Primary Neuronal Culture and Magnetofection

Cortices from E15.5 mouse embryos were dissected in Hank's buffered salt solution (HBSS) supplemented with HEPES (pH 7.4; 2.5 mM), $CaCl_2$ (1 mM, Sigma), $MgSO_4$ (1 mM, Sigma), $NaHCO_3$ (4 mM, Sigma), and D-glucose (30 mM, Sigma), hereafter referred to as cHBSS. Cortices were dissociated in cHBSS containing papain (Worthington) and DNase I (100 μg/ml, Sigma) for 20 min at 37°C, washed three times, and manually triturated in cHBSS supplemented with DNase. Cells were then plated at 5.0×10^4 cells per 35 mm glass bottom dish (Matek) coated with poly-D-lysine (1 mg/ml, Sigma) and cultured for 5–7 days in Neurobasal medium supplemented with B27 (1×), N2 (1×), L-glutamine (2 mM), and penicillin (5 units/ml)-streptomycin (50 mg/ml). To transfect cultured neurons, we performed magnetofection using NeuroMag (OZ Bioscience) according to the manufacturer's protocol. Live imaging was performed in cHBSS (see Supplemental Information for details).

Image Acquisition and Analysis

Images were acquired with a Nikon A1R confocal, whereas Movies S1, S2, S3, S4, S5, and S6 were acquired with an Andor iXon 897 CCD camera on a Nikon Ti-E microscope. Dual imaging of Mito-DsRED and VGLUT1-Venus was acquired at 1 frame per 10 s for 30 min for Figures 4, 5, 6, and 7. See Supplemental Information for details.

Western Blotting

Western blotting was carried out as described in Williams et al. (2011). See Supplemental Information for details.

In Situ Hybridization

In situ hybridization was carried out using digoxigenin-labeled riboprobes at the In Situ Hybridization Core Facility from University of North Carolina at Chapel Hill. Probes were generated from the following mouse complementary DNA (cDNA) clones purchased from Open Biosystems (Huntsville, AL): NUAK1 (GenBank: CB522124; IMAGE: 6842317) and NUAK2 (GenBank: CB248251; IMAGE: 5718428).

Quantifications and Statistics

Axon tracing and measurements were performed with NIS-Elements software (Nikon). Signal intensity measurements were performed using ImageJ. Statistical analyses were performed with Prism (GraphPad Software). Statistical tests performed are included in each figure legend.

Constructs, Time-Lapse Imaging, Immunocytochemistry, NUAK1 In Vitro Kinase Assay, and RT-PCR Assays

See Supplemental Information for details.

SUPPLEMENTAL INFORMATION

Supplemental Information includes Extended Experimental Procedures, seven figures, and six movies and can be found with this article online at http://dx.doi.org/10.1016/j.cell.2013.05.021.

ACKNOWLEDGMENTS

The authors would like to thank members of the Polleux lab and Sandra Encalada for useful discussions. We thank Kathy Spencer for excellent help with microscopy and Trevor Sauerbrey for technical help. We would also like to thank Brendan Lilley, Ulrich Müller, Anton Maximov, and Sandra Encalada for critical reading of the manuscript. We thank Joshua Sanes, Zu-Hang Shen, Ulrich Müller, Etienne Herzog, and Don Arnold for sharing reagents. This work was funded by NIH R01AG031524 (F.P.), ADI-Novartis funds (F.P.), Fondation pour la Recherche Medicale (J.C.), Philippe Foundation (J.C.), and NIH 5F32NS080464 (T.L.). J.C, T.L., and F.P. conceived the experiments and interpreted the results, and J.C., T.L., S.L., V.C., and D.-Y.L. performed the experiments. S.A. provided the NUAK1 knockout mice. J.C., T.L., and F.P. prepared the manuscript.

Received: October 19, 2012
Revised: April 1, 2013
Accepted: May 8, 2013
Published: June 20, 2013

REFERENCES

Alessi, D.R., Sakamoto, K., and Bayascas, J.R. (2006). LKB1-dependent signaling pathways. Annu. Rev. Biochem. *75*, 137–163.

Amato, S., Liu, X., Zheng, B., Cantley, L., Rakic, P., and Man, H.Y. (2011). AMP-activated protein kinase regulates neuronal polarization by interfering with PI 3-kinase localization. Science *332*, 247–251.

Baas, A.F., Kuipers, J., van der Wel, N.N., Batlle, E., Koerten, H.K., Peters, P.J., and Clevers, H.C. (2004). Complete polarization of single intestinal epithelial cells upon activation of LKB1 by STRAD. Cell *116*, 457–466.

Bardeesy, N., Sinha, M., Hezel, A.F., Signoretti, S., Hathaway, N.A., Sharpless, N.E., Loda, M., Carrasco, D.R., and DePinho, R.A. (2002). Loss of the Lkb1 tumour suppressor provokes intestinal polyposis but resistance to transformation. Nature *419*, 162–167.

Barnes, A.P., and Polleux, F. (2009). Establishment of axon-dendrite polarity in developing neurons. Annu. Rev. Neurosci. *32*, 347–381.

Barnes, A.P., Lilley, B.N., Pan, Y.A., Plummer, L.J., Powell, A.W., Raines, A.N., Sanes, J.R., and Polleux, F. (2007). LKB1 and SAD kinases define a pathway required for the polarization of cortical neurons. Cell *129*, 549–563.

Brickley, K., and Stephenson, F.A. (2011). Trafficking kinesin protein (TRAK)-mediated transport of mitochondria in axons of hippocampal neurons. J. Biol. Chem. *286*, 18079–18092.

Figure 7. LKB1 and NUAK1 Are Necessary and Sufficient for Mitochondrial Immobilization at Nascent Presynaptic Sites

(A, C, and E) Representative dual color kymographs of axonal VGLUT1-Venus puncta and mitochondria dynamics in cortical neurons electroporated with the indicated constructs.

(B, D, and F) Overlapping pixels maps of (A), (C), and (E) were created in Fiji/ImageJ using the Colocalization Threshold program.

(G) Schematic illustration of the parameters used to quantify the results shown in (H)–(K).

(H) Knockdown of LKB1 or NUAK1 decreased the dwell time of mitochondria over nascent presynaptic sites, whereas overexpression of LKB1 or NUAK1 increased it.

(I) Knockdown of LKB1 or NUAK1 did not affect the dwell time of mitochondria outside nascent presynaptic sites, whereas overexpression of LKB1 or NUAK1 slightly decreased it.

(J) Knockdown or overexpression of LKB1 and NUAK1 do not affect the linear density of stable (for 30 min) VGLUT1-Venus nascent presynaptic sites.

(K) Loss of LKB1 or NUAK1 decreased, whereas overexpression of LKB1 or NUAK1 increased the percentage of mitochondria stably captured (for 30 min) at presynaptic sites.

Data represent average value ± SEM (H–K). Statistical analysis: Mann-Whitney test. See also Figure S7.

Crump, J.G., Zhen, M., Jin, Y., and Bargmann, C.I. (2001). The SAD-1 kinase regulates presynaptic vesicle clustering and axon termination. Neuron *29*, 115–129.

Donahoo, A.L., and Richards, L.J. (2009). Understanding the mechanisms of callosal development through the use of transgenic mouse models. Semin. Pediatr. Neurol. *16*, 127–142.

Franco, S.J., Martinez-Garay, I., Gil-Sanz, C., Harkins-Perry, S.R., and Müller, U. (2011). Reelin regulates cadherin function via Dab1/Rap1 to control neuronal migration and lamination in the neocortex. Neuron *69*, 482–497.

Gallo, G. (2011). The cytoskeletal and signaling mechanisms of axon collateral branching. Dev. Neurobiol. *71*, 201–220.

Goebbels, S., Bormuth, I., Bode, U., Hermanson, O., Schwab, M.H., and Nave, K.A. (2006). Genetic targeting of principal neurons in neocortex and hippocampus of NEX-Cre mice. Genesis *44*, 611–621.

Gorski, J.A., Talley, T., Qiu, M., Puelles, L., Rubenstein, J.L., and Jones, K.R. (2002). Cortical excitatory neurons and glia, but not GABAergic neurons, are produced in the Emx1-expressing lineage. J. Neurosci. *22*, 6309–6314.

Hall, A., and Lalli, G. (2010). Rho and Ras GTPases in axon growth, guidance, and branching. Cold Spring Harb. Perspect. Biol. *2*, a001818.

Hand, R., and Polleux, F. (2011). Neurogenin2 regulates the initial axon guidance of cortical pyramidal neurons projecting medially to the corpus callosum. Neural Dev. *6*, 30.

Hand, R., Bortone, D., Mattar, P., Nguyen, L., Heng, J.I., Guerrier, S., Boutt, E., Peters, E., Barnes, A.P., Parras, C., et al. (2005). Phosphorylation of Neurogenin2 specifies the migration properties and the dendritic morphology of pyramidal neurons in the neocortex. Neuron *48*, 45–62.

Harris, K.M., and Weinberg, R.J. (2012). Ultrastructure of synapses in the mammalian brain. Cold Spring Harb. Perspect. Biol. *4*, a005587.

Herzog, E., Nadrigny, F., Silm, K., Biesemann, C., Helling, I., Bersot, T., Steffens, H., Schwartzmann, R., Nagerl, U.V., El Mestikawy, S., et al. (2011). In vivo imaging of intersynaptic vesicle exchange using VGLUT1 Venus knock-in mice. J. Neurosci. *31*, 15544–15559.

Hirano, M., Kiyonari, H., Inoue, A., Furushima, K., Murata, T., Suda, Y., and Aizawa, S. (2006). A new serine/threonine protein kinase, Omphk1, essential to ventral body wall formation. Dev. Dyn. *235*, 2229–2237.

Huber, A.B., Kolodkin, A.L., Ginty, D.D., and Cloutier, J.F. (2003). Signaling at the growth cone: ligand-receptor complexes and the control of axon growth and guidance. Annu. Rev. Neurosci. *26*, 509–563.

Inoue, E., Mochida, S., Takagi, H., Higa, S., Deguchi-Tawarada, M., Takao-Rikitsu, E., Inoue, M., Yao, I., Takeuchi, K., Kitajima, I., et al. (2006). SAD: a presynaptic kinase associated with synaptic vesicles and the active zone cytomatrix that regulates neurotransmitter release. Neuron *50*, 261–275.

Jaleel, M., McBride, A., Lizcano, J.M., Deak, M., Toth, R., Morrice, N.A., and Alessi, D.R. (2005). Identification of the sucrose non-fermenting related kinase SNRK, as a novel LKB1 substrate. FEBS Lett. *579*, 1417–1423.

Jeanneteau, F., Deinhardt, K., Miyoshi, G., Bennett, A.M., and Chao, M.V. (2010). The MAP kinase phosphatase MKP-1 regulates BDNF-induced axon branching. Nat. Neurosci. *13*, 1373–1379.

Kalil, K., Szebenyi, G., and Dent, E.W. (2000). Common mechanisms underlying growth cone guidance and axon branching. J. Neurobiol. *44*, 145–158.

Kang, J.S., Tian, J.H., Pan, P.Y., Zald, P., Li, C., Deng, C., and Sheng, Z.H. (2008). Docking of axonal mitochondria by syntaphilin controls their mobility and affects short-term facilitation. Cell *132*, 137–148.

Kemphues, K.J., Priess, J.R., Morton, D.G., and Cheng, N.S. (1988). Identification of genes required for cytoplasmic localization in early C. elegans embryos. Cell *52*, 311–320.

Kishi, M., Pan, Y.A., Crump, J.G., and Sanes, J.R. (2005). Mammalian SAD kinases are required for neuronal polarization. Science *307*, 929–932.

Lee, J.H., Koh, H., Kim, M., Kim, Y., Lee, S.Y., Karess, R.E., Lee, S.H., Shong, M., Kim, J.M., Kim, J., and Chung, J. (2007). Energy-dependent regulation of cell structure by AMP-activated protein kinase. Nature *447*, 1017–1020.

Lizcano, J.M., Göransson, O., Toth, R., Deak, M., Morrice, N.A., Boudeau, J., Hawley, S.A., Udd, L., Mäkelä, T.P., Hardie, D.G., and Alessi, D.R. (2004). LKB1 is a master kinase that activates 13 kinases of the AMPK subfamily, including MARK/PAR-1. EMBO J. *23*, 833–843.

Martin, S.G., and St Johnston, D. (2003). A role for Drosophila LKB1 in anterior-posterior axis formation and epithelial polarity. Nature *421*, 379–384.

Meyer, M.P., and Smith, S.J. (2006). Evidence from in vivo imaging that synaptogenesis guides the growth and branching of axonal arbors by two distinct mechanisms. J. Neurosci. *26*, 3604–3614.

Mian, I., Pierre-Louis, W.S., Dole, N., Gilberti, R.M., Dodge-Kafka, K., and Tirnauer, J.S. (2012). LKB1 destabilizes microtubules in myoblasts and contributes to myoblast differentiation. PLoS ONE *7*, e31583.

Mirouse, V., Swick, L.L., Kazgan, N., St Johnston, D., and Brenman, J.E. (2007). LKB1 and AMPK maintain epithelial cell polarity under energetic stress. J. Cell Biol. *177*, 387–392.

Mizuno, H., Hirano, T., and Tagawa, Y. (2007). Evidence for activity-dependent cortical wiring: formation of interhemispheric connections in neonatal mouse visual cortex requires projection neuron activity. J. Neurosci. *27*, 6760–6770.

Mizuno, H., Hirano, T., and Tagawa, Y. (2010). Pre-synaptic and post-synaptic neuronal activity supports the axon development of callosal projection neurons during different post-natal periods in the mouse cerebral cortex. Eur. J. Neurosci. *31*, 410–424.

Nishimura, Y., Applegate, K., Davidson, M.W., Danuser, G., and Waterman, C.M. (2012). Automated screening of microtubule growth dynamics identifies MARK2 as a regulator of leading edge microtubules downstream of Rac1 in migrating cells. PLoS ONE *7*, e41413.

Polleux, F., and Snider, W. (2010). Initiating and growing an axon. Cold Spring Harb. Perspect. Biol. *2*, a001925.

Ruthazer, E.S., Li, J., and Cline, H.T. (2006). Stabilization of axon branch dynamics by synaptic maturation. J. Neurosci. *26*, 3594–3603.

Sabo, S.L., Gomes, R.A., and McAllister, A.K. (2006). Formation of presynaptic terminals at predefined sites along axons. J. Neurosci. *26*, 10813–10825.

Schon, E.A., and Przedborski, S. (2011). Mitochondria: the next (neurode)generation. Neuron *70*, 1033–1053.

Shelly, M., Cancedda, L., Heilshorn, S., Sumbre, G., and Poo, M.M. (2007). LKB1/STRAD promotes axon initiation during neuronal polarization. Cell *129*, 565–577.

Sheng, Z.H., and Cai, Q. (2012). Mitochondrial transport in neurons: impact on synaptic homeostasis and neurodegeneration. Nat. Rev. Neurosci. *13*, 77–93.

Takeda, S., Yamazaki, H., Seog, D.H., Kanai, Y., Terada, S., and Hirokawa, N. (2000). Kinesin superfamily protein 3 (KIF3) motor transports fodrin-associating vesicles important for neurite building. J. Cell Biol. *148*, 1255–1265.

Uesaka, N., Ruthazer, E.S., and Yamamoto, N. (2006). The role of neural activity in cortical axon branching. Neuroscientist *12*, 102–106.

Vos, M., Lauwers, E., and Verstreken, P. (2010). Synaptic mitochondria in synaptic transmission and organization of vesicle pools in health and disease. Front. Synaptic Neurosci. *2*, 139.

Walsh, C.A., Morrow, E.M., and Rubenstein, J.L. (2008). Autism and brain development. Cell *135*, 396–400.

Wang, C.L., Zhang, L., Zhou, Y., Zhou, J., Yang, X.J., Duan, S.M., Xiong, Z.Q., and Ding, Y.Q. (2007). Activity-dependent development of callosal projections in the somatosensory cortex. J. Neurosci. *27*, 11334–11342.

Wang, X., Winter, D., Ashrafi, G., Schlehe, J., Wong, Y.L., Selkoe, D., Rice, S., Steen, J., LaVoie, M.J., and Schwarz, T.L. (2011). PINK1 and Parkin target Miro

for phosphorylation and degradation to arrest mitochondrial motility. Cell *147*, 893–906.

Watts, J.L., Morton, D.G., Bestman, J., and Kemphues, K.J. (2000). The C. elegans par-4 gene encodes a putative serine-threonine kinase required for establishing embryonic asymmetry. Development *127*, 1467–1475.

Williams, T., Courchet, J., Viollet, B., Brenman, J.E., and Polleux, F. (2011). AMP-activated protein kinase (AMPK) activity is not required for neuronal development but regulates axogenesis during metabolic stress. Proc. Natl. Acad. Sci. USA *108*, 5849–5854.

Yu, C.R., Power, J., Barnea, G., O'Donnell, S., Brown, H.E., Osborne, J., Axel, R., and Gogos, J.A. (2004). Spontaneous neural activity is required for the establishment and maintenance of the olfactory sensory map. Neuron *42*, 553–566.

Zagórska, A., Deak, M., Campbell, D.G., Banerjee, S., Hirano, M., Aizawa, S., Prescott, A.R., and Alessi, D.R. (2010). New roles for the LKB1-NUAK pathway in controlling myosin phosphatase complexes and cell adhesion. Sci. Signal. *3*, ra25.

Zoghbi, H.Y., and Bear, M.F. (2012). Synaptic dysfunction in neurodevelopmental disorders associated with autism and intellectual disabilities. Cold Spring Harb. Perspect. Biol. *4*, a009886.

Cell

EXTENDED EXPERIMENTAL PROCEDURES

Constructs

The empty vector pCAG-CRE-IRES-GFP (pCIG2) and CRE expressing pCIG2-CRE vectors (Hand et al., 2005), pCIG2-SAD-B (Barnes et al., 2007) and AMPKα2 (Williams et al., 2011), and CAG-mVENUS expressing vector pSCV2 (Hand and Polleux, 2011) have been described previously. Wild-type mouse LKB1 cDNA was cloned into pCMV-Tag3B vector (Stratagene) between KpnI and EcoRI sites. A XhoI site was inserted upstream of Myc tag with Quickchange II site-directed mutagenesis kit (Stratagene), then myc-LKB1 was transferred into pCIG2 between XhoI and EcoRI sites. Kinase-dead (KD) LKB1 was generated by replacing K78 residue by alanine (K78A) by site-directed mutagenesis of pCMV-myc-mLKB1. pCAG HA-LKB1 was cloned by inserting the DNA encoding a hemagglutinin (HA) tag 5′ to the DNA encoding mouse *lkb1* downstream of the CAG promoter via PCR. Flag tagged Mouse NUAK1 cDNA was amplified by PCR from image clone 30355405 (accession number BC082328; Open Biosystems) then inserted into pCIG2 vector between XhoI and EcoRI sites. HA-tagged mouse NUAK2 was amplified by PCR from image clone 6816569 (accession number BC046833; Open Biosystems), then cloned into a modified version of pCIG2 with a ligation-independent cloning strategy (pCIG2-LIC). pCAG-mitoDsRED1 was created by placing the DNA encoding DsRED1-Mito (from pDsRED1-Mito; Clontech) 3′ to the CAG promoter using PCR. EGFP-SyntaphilinFL and EGFP-SyntaphilinΔMTB were cloned 3′ to the CAG promoter by cutting the original constructs from Zu-Hang Shen (Kang et al., 2008) with Age1 and BamH1 to create pCAG-EGFP-SyntaphilinFL and pCAG-EGFP-SyntaphilinΔMTB. pCAG-HAmCherry was created by PCR of the DNA encoding HAmCherry 3′ to the CAG promoter. pCMV-EB3-EGFP was created by PCR of *eb3* from mouse cDNA and insertion 3′ to pEGFP-C1. pCIG2-ms SNPH was created by PCR of mouse *snph* from mouse cDNA and insertion 3′ to the CAG promoter. pDCX-CRE-iGFP, VGLUT1-Venus, and pCMV-HA-mCherry were generous gifts from Ulrich Müller (Franco et al., 2011), Etienne Herzog (Herzog et al., 2011), and Don Arnold (Lewis et al., 2011), respectively.

shRNA Vectors

Empty vector pLKO.1 and shRNA targeting plasmids toward mouse LKB1 (shLKB1_3: TRC0000024146 and shLKB1_5: TRC0000024148), mouse NUAK1 (shNUAK1_1: TRC0000024112 and shNUAK1_2: TRC0000024113) and mouse NUAK2 (shNUAK2_1: TRC0000024270 and shNUAK2_2: TRC0000024271) were selected from The RNAi Consortium shRNA Library (TRC) from the Broad Institute and obtained from the Lentiviral Core Facility (Gene Therapy Center) from the University of North Carolina. Plasmids containing the shRNA against mouse SNPH (shSNPH_1: TRC0000201826 and shSNPH_2: TRC0000201959) from the TRC library were purchased from OpenBioSystems. The following Plasmids containing shRNAs against SAD-A and SAD-B in pSM2c and pPRIME-CMV-GFP backbones and corresponding control vectors were kind gifts of Joshua Sanes (Harvard University). Unless stated otherwise shRNA plasmids targeting a same gene were pooled at a 1:1 ratio and used at the final concentration of 1 μg/μL for in utero cortical electroporation or ex vivo electroporation.

Ex Vivo Electroporation

Briefly, electroporation of dorsal telencephalic progenitors was performed by injecting plasmid DNA (1-2 μg/μl endotoxin-free plasmid DNA; Midi or Maxi prep kit from Macherey-Nagel) plus 0.5% Fast Green (Sigma; 1:20 ratio) using the MicroInject-1000 (BTX) microinjector into the lateral ventricles of isolated E15.5 embryonic mouse heads that were decapitated and placed in complete HBSS (Polleux and Ghosh, 2002). Electroporations were performed on the whole head (skin and skull intact) with gold-coated electrodes (GenePads 5 × 7 mm BTX) using an ECM 830 electroporator (BTX) and the following parameters: Five 100 ms long pulses separated by 100 ms long intervals at 20 V. Immediately after electroporation, the brain was extracted and prepared as stated in the neuronal culture section below.

Dual Channel Imaging of Nascent Presynaptic Sites and Mitochondria

Ex utero electroporation was performed at E15.5 in either *LKB1*$^{F/F}$ or C57Bl6 time pregnant mice with the constructs indicated: for *LKB1*$^{F/F}$ – pCAG:empty or pCAG:CRE with pCAG:VGLUT1-Venus, and mitoDsRED1; for C57Bl6 – pLKO:control shRNA, pLKO:NUAK1 shRNA or pLKO:LKB1 shRNA with VGLUT1-EGFP, and mitoDsRED1; LKB1 or NUAK1 overexpression – pCAG:empty, pCAG:Myc-NUAK1 or pCAG:HA-LKB1 with pCAG:VGLUT1-EGFP, and pCAG:mitoDsRED1. Neurons were then cultured as previously stated until 7DIV. Imaging was performed at 7DIV in cHBSS with a 60x objective and the microscope at 1.5x. Videos were acquired at 0.1 fps for 30 min. Dual channel kymographs were created in NIS Elements by drawing a line along the imaged axon shaft. These kymographs were then analyzed for mitochondrial and VGLUT1 dynamics using NIS Elements. The Colocalization Threshold program in FUJI/ImageJ was used to create the overlapping pixel maps.

EB3-EGFP-Based Microtubule Dynamics

Dissociated cultures were made as previously described from E15.5 C57Bl6 embryos with the exception that the dishes were coated with 8 μg/ml L1 (R&D) to promote growth cone formation. At 3DIV, neurons were magnetofected using NeuroMag, the standard transfection protocol from Ozbiosciences, and the indicated plasmids: pLKO empty or pLKO NUAK1 shRNA, pCAG HA-mCherry and pCMV EB3-EGFP. At 5DIV, transfected neurons were imaged in cHBSS with a 60x objective and the microscope at 1.5x. Videos

were acquired at 0.5fps for 5 min. Growth cones were analyzed for area and area explored by microtubules using FUJI/ImageJ. EB3 comets were tracked using the 2D tracking module of NIS Elements.

Immunocytochemistry and Immunohistochemistry

Cells were fixed for 15 min at room temperature in 4% (w/v) paraformaldehyde in PBS, and incubated for 1 hr in 0.1% Triton X-100, 1% BSA (Sigma), 5% Normal Goat Serum in PBS to permeabilize and block nonspecific staining. Primary and secondary antibodies were diluted in the buffer described above. Primary antibodies were incubated overnight at 4°C and secondary antibodies were incubated for 1 hr at room temperature. Coverslips were mounted on slides with Fluoromount G (EMS). Primary antibodies used for immunohistochemistry and immunocytochemistry in this study are chicken anti-GFP (5 μg/ml, Aves Lab), mouse anti-TAG1 (1:100, Developmental Studies Hybridoma Bank), mouse anti-Synaptobrevin2 (1:2,000, Synaptic Systems), mouse anti-Bassoon (1:500, ENZO life sciences), rabbit anti-activated Caspase-3 (1:500, Cell Signaling), rabbit anti-CUX1 (1:500, Santa Cruz), rabbit anti-MAP2 (1:1,000, Millipore), rabbit anti-Syntaphilin (1:100, Santa Cruz (H-250)), rabbit anti-Synapsin1 (1:1,000, Synaptic Systems), rat anti-CTIP2 (1:2,000, AbCAM). All secondary antibodies were Alexa-conjugated (Invitrogen) and used at a 1:1000 dilution. Nuclear DNA was stained using Hoechst 33258 (1:10,000, Pierce).

Western Blotting

Cells were harvested in cold DPBS and lysed in ice-cold lysis buffer containing 25 mM Tris (pH7.5), 2 mM $MgCl_2$, 600 mM NaCl, 2 mM EDTA, 0.5% NP-40, 1X protease and phosphatase cocktail inhibitors (Sigma) and Benzonase (0.25 U/μl of lysis buffer; Novagen). Aliquots of the proteins were separated by SDS-PAGE and then transferred to a polyvinylidene difluoride (PVDF) membrane (Amersham). After transfer, the membrane was washed 3X in Tris Buffer Saline (10 mM Tris-HCl pH 7.4, 150 mM NaCl) with 0.1% of Tween 20 (T-TBS), blocked for 1 hr at room temperature in 5% milk in T-TBS, followed by 4°C overnight incubation with the appropriate primary antibody in 5% milk-T-TBS. The following day, the membrane was washed 3X in T-TBS, incubated at room temperature for 1 hr with HRP-coupled secondary antibodies (Invitrogen) at 1:10,000 dilution in 5% milk-T-TBS, followed by 3X T-TBS washes. Visualization was performed by quantitative chemiluminescence using a Fluorochem Q imager (ProteinSimple). Signal intensity was quantified using AlphaView software (ProteinSimple). Primary antibodies used for Western-blotting are mouse anti-Flag (1:5,000, SIGMA), mouse anti-Myc (1:2,000, Roche (9E10)), mouse anti-HA (1:2,000, Covance), mouse anti-LKB1 (1:1,000, SIGMA), mouse anti-ERK (p42-44) (1:2,000, Cell Signaling), mouse anti-Actin (1:15,000, Millipore), mouse anti-Tyrosinated tubulin (1:5,000, SIGMA), mouse anti-Acetylated tubulin (1:5,000, SIGMA), mouse anti-tubulin (1:5,000, SIGMA), rabbit anti-NUAK1 (1:1,000, Cell Signaling), rabbit anti-NUAK2 (1:1,000, Cell Signaling) and rabbit anti-SNPH (1:1,000, Santa-Cruz).

NUAK1 Kinase Activity

NUAK1 kinase activity was assessed as described elsewhere (Zagórska et al., 2010) with minor modification. Nex^{Cre};LKB1 cKO neurons were cultured as described above and lysed at 7DIV in NP-40 buffer (20 mM Tris pH 7.5, 150 mM NaCl, 2 mM EDTA, 1% NP-40, 1X protease and phosphatase cocktail inhibitors). 200 μg of proteins were diluted in 1 ml of NP-40 buffer and immunoprecipitated with 2 μl of anti-NUAK1 antibody overnight at 4°C. The subsequent day, 50 μl of protein A/G-agarose (Roche) was added to the lysate for 1 hr at 4°C. Agarose bead were then washed 5 times with 1 ml of NP-40 buffer, then once with 1 ml of Assay buffer (50 mM Tris pH 7.5, 150 mM NaCl, 10 mM $MgCL_2$, 0.1 mM EGTA, 1 mM DTT). Agarose beads were incubated with the peptide substrate CHKtide (200 μM) (Millipore) in presence of 0.1 mM γ^{32}P-ATP in 50 μl of Assay buffer at 30°C. After 30 min, the supernatant was applied onto P81 phosphocellulose paper (Millipore) and washed 5 times in phosphoric acid, and once in acetone. Radioactivity was quantified by Cherenkov counting.

Image Acquisition and Analyses

Confocal images were acquired in 1024x1024 mode with a Nikon Ti-E microscope equipped with the A1R laser scanning confocal microscope using the Nikon software NIS-Elements (Nikon Corporation, Melville, NY). We used the following objective lenses (Nikon): 10x PlanApo; NA 0.45, 20x PlanApo VC; NA 0.75, 60x Apo TIRF; NA 1.49. Time-lapse images were acquired in 512x512 mode with a Nikon Ti-E microscope equipped with an EM-CCD Andor iXon3 897 Camera using the Nikon software NIS-Elements. Mitochondria were imaged at 0.1 frames per second for 30 min, VGLUT1 vesicles were imaged at 1.33 frames per second for 3-5 min (Figure S6) or 0.1 frames per second for 30 min (Figure 7), and EB3 comets were imaged at 0.5 frames per second for 5 min. Live imaging of axonal branching of 5DIV neurons was performed over 15 hr at 1 frame every 5 min. Live imaging of mitochondria, VGLUT1 and EB3 was done with the 60x Apo TIRF; NA 1.49 objective, while live imaging of branching was done with the 10x PlanApo; NA 0.45 objective. Imaging of axons at 60x was concentrated on the axon shaft with avoidance of both the proximal and distal 1/3 of the axon unless stated otherwise. These regions were avoided because mitochondrial trafficking appears to be highly variable in these regions. Live imaging was done in the Tokai Hit chamber system with the following settings: top heater – 37°C, Bottom heater - 40°C, Bath heater - 37°C, Objective heater - 37°C, CO_2 – 125 ml/min of 5% CO_2, 21.4% O_2, 73.6% N_2. Analysis and tracking of confocal and time-lapse images was performed with NIS-Elements software. Kymographs were created with either NIS-Elements or ImageJ 1.44p with the ImageJ Kymograph plugin (J. Rietdorf and A. Seitz).

Expression Time Course and RT-PCR

Cortex from C57Bl/6J mice were collected at the indicated ages and either lysed with protein lysis buffer (see above) or for total RNA extraction using the Nucleospin RNA II kit (Macherey-Nagel). cDNA synthesis was performed from 1 μg RNA using SuperScript III (Invitrogen) and primed with random hexamers. RT-PCR was performed using Taq DNA polymerase (New England Biolabs). Quantitative-RT-PCR (Q-RT-PCR) was performed using the RotorGene RG-3000 thermocycler (Corbett Research) and GoTaq qPCR mastermix (Promega). The primers used were: mNUAK1_RT_F (GATCAGCAGCGGAGAGTACC) and mNUAK1_RT_R (TCGA TAAAGCCAGTGCTGTG) for NUAK1, and mNUAK2_RT_F (AAGGTGAAGAAGGCACGAGA) and mNUAK2_RT_R (ACTATCT CAGGCGAGGCGTA) for NUAK2.

Statistical Analysis

Data are a minimum of three independent experiments unless stated otherwise. Figure 2: N numbers for (I) N_{WT} = 11, N_{HET} = 4, N_{KO} = 6. Figure 3: N numbers for (G-I) $N_{control}$: 513 neurons, N_{LKB1}:141, $N_{NUAK1/2}$:151, N_{NUAK1}:314, $N_{LKB1+NUAK1}$:102. (J-K) $N_{control}$:449, $N_{LKB1\text{-}OE}$:219, $N_{NUAK1\text{-}OE}$:328, $N_{NUAK1sh}$:143, $N_{NUAK1sh+LKB1\text{-}OE}$:151, N_{LKB1sh}:116, $N_{LKB1sh+NUAK1\text{-}OE}$:190. Figure 4: N numbers for (G-K) N_{NexWT}: 280 mitochondria from 10 axons, N_{NexKO}: 290 mitochondria from 11 axons, $N_{NUAK1\ WT}$: 135 from 6 axons, $N_{NUAK1\ KO}$: 144 from 6 axons, N_{EGFP}: 364 from 12 axons, $N_{LKB1\ WT}$: 241 from 10 axons, $N_{NUAK1\ WT}$: 100 from 6 axons. Figure 5: N number for mitochondria trafficking $N_{Control}$ shRNA:228 mitochondria from 12 axons; N_{snph} shRNA:239/12; N_{SNPH}: 179/8; $N_{SNPH\text{-}\Delta MTB}$: 292/10. N number for axon branching $N_{Control}$ shRNA: 179 neurons; N_{snph} shRNA: 137; N_{SNPH}: 173; $N_{SNPH\text{-}\Delta MTB}$: 173. Figure 6: N number for mitochondrial trafficking: $N_{EGFP\ in\ K}$ = 214 mitochondria from 8 axons, $N_{CAG::Cre}$: 182 mitochondria from 6 axons, $N_{CAG::Cre\ +\ SNPH}$: 200 /9. $N_{EGFP\ in\ M}$:200/7, N_{LKB1WT}: 212/8 axons, $N_{LKB1WT\ +\ SNPH\text{-}\Delta MTB}$: 163/7. N number for axon branching: $N_{EGFP\ in\ L}$:153 neurons, $N_{CAG::Cre}$:151, N_{SNPH}:173, $N_{CAG::Cre\ +\ SNPH}$:147. $N_{EGFP\ in\ N}$:183, N_{LKB1WT}:157, $N_{LKB1WT\ +\ SNPH\text{-}\Delta MTB}$:172. Figure 7: N number for mitochondrial trafficking $N_{Control\ shRNA}$ = 95 dwelling, 89 stationary mitochondria from 18 axons, $N_{LKB1\ shRNA}$:100/38/16, $N_{NUAK1\ shRNA}$: 83/54/12, $N_{Control}$ = 45/81/17, $N_{LKB1\ WT}$:49/110/15, $N_{NUAK1\ WT}$:26/38/10.

SUPPLEMENTAL REFERENCES

Lewis, T.L., Jr., Mao, T., and Arnold, D.B. (2011). A role for myosin VI in the localization of axonal proteins. PLoS Biol. *9*, e1001021.

Polleux, F., and Ghosh, A. (2002). The slice overlay assay: a versatile tool to study the influence of extracellular signals on neuronal development. Sci. STKE *2002*, pl9.

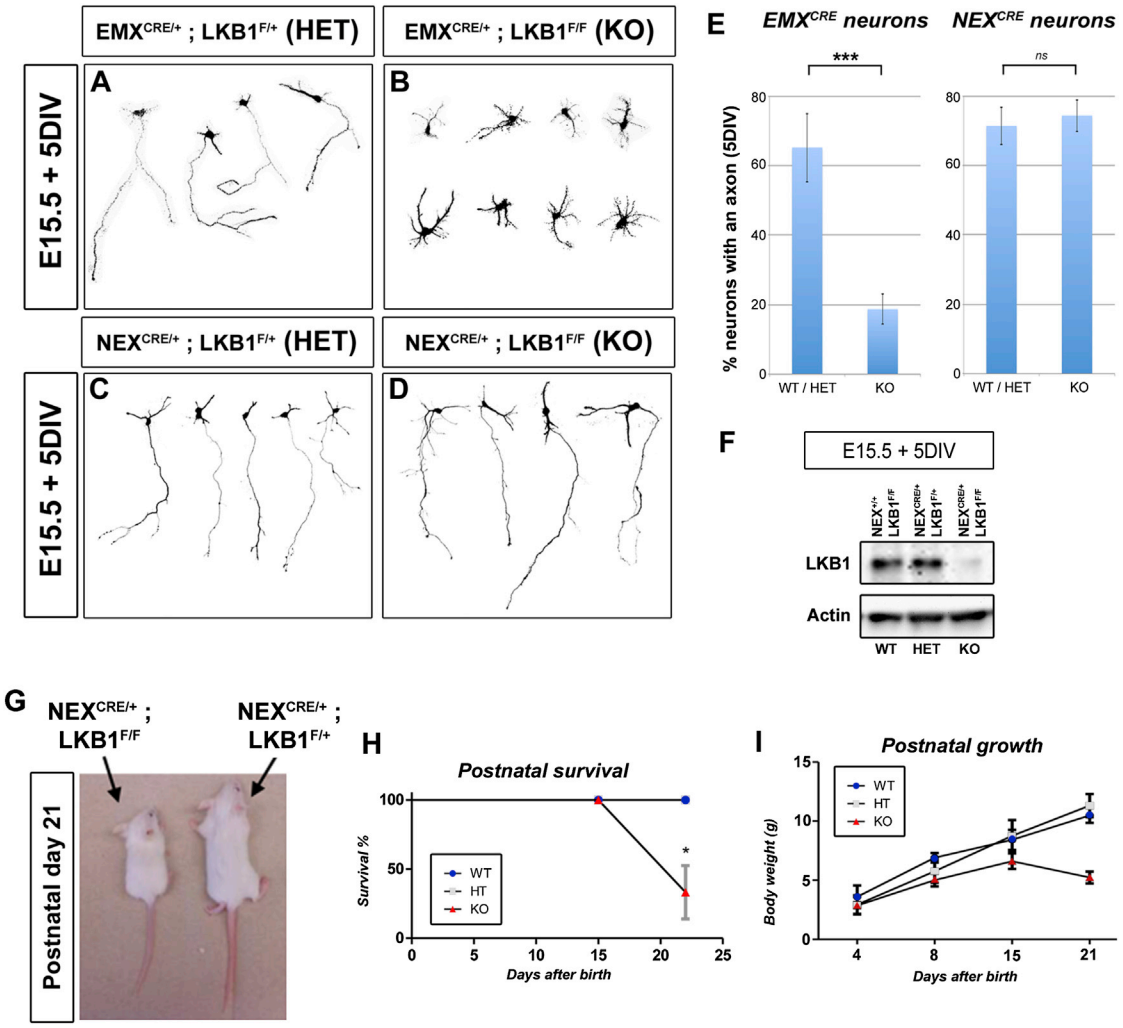

Figure S1. Phenotype of NEX^{Cre} Conditional LKB1 Knockout Mice, Related to Figure 1

(A–D) Representative cortical neurons from dissociated cultures isolated from Emx1^{Cre};LKB1 (A-B) and NEX^{Cre};LKB1 (C-D) embryos after 5 DIV. Ex vivo cortical electroporation with a Venus expressing plasmid and cortex dissociation was performed at E15.5.

(E) Quantification of neuron polarization after 5DIV relative to neurons in (A-D). Axon is defined by a neurite of length > 100 μm and positive for the axonal marker SMI312. Average ± SEM.

(F) Expression of LKB1 proteins in WT, HET and cKO NEX^{Cre};LKB1 neurons. Western-blot analysis was performed with the indicated antibodies. Actin was used as a loading control.

(G) Comparison of body size difference between conditional heterozygous (HET; right) and conditional homozygous knockout (KO; left) NEX^{Cre};LKB1 mice at age P21.

(H and I) Postnatal survival curve of NEX^{Cre};LKB1 mice from birth to P21 (H) and postnatal body weight growth curve (I). Average ± SEM.

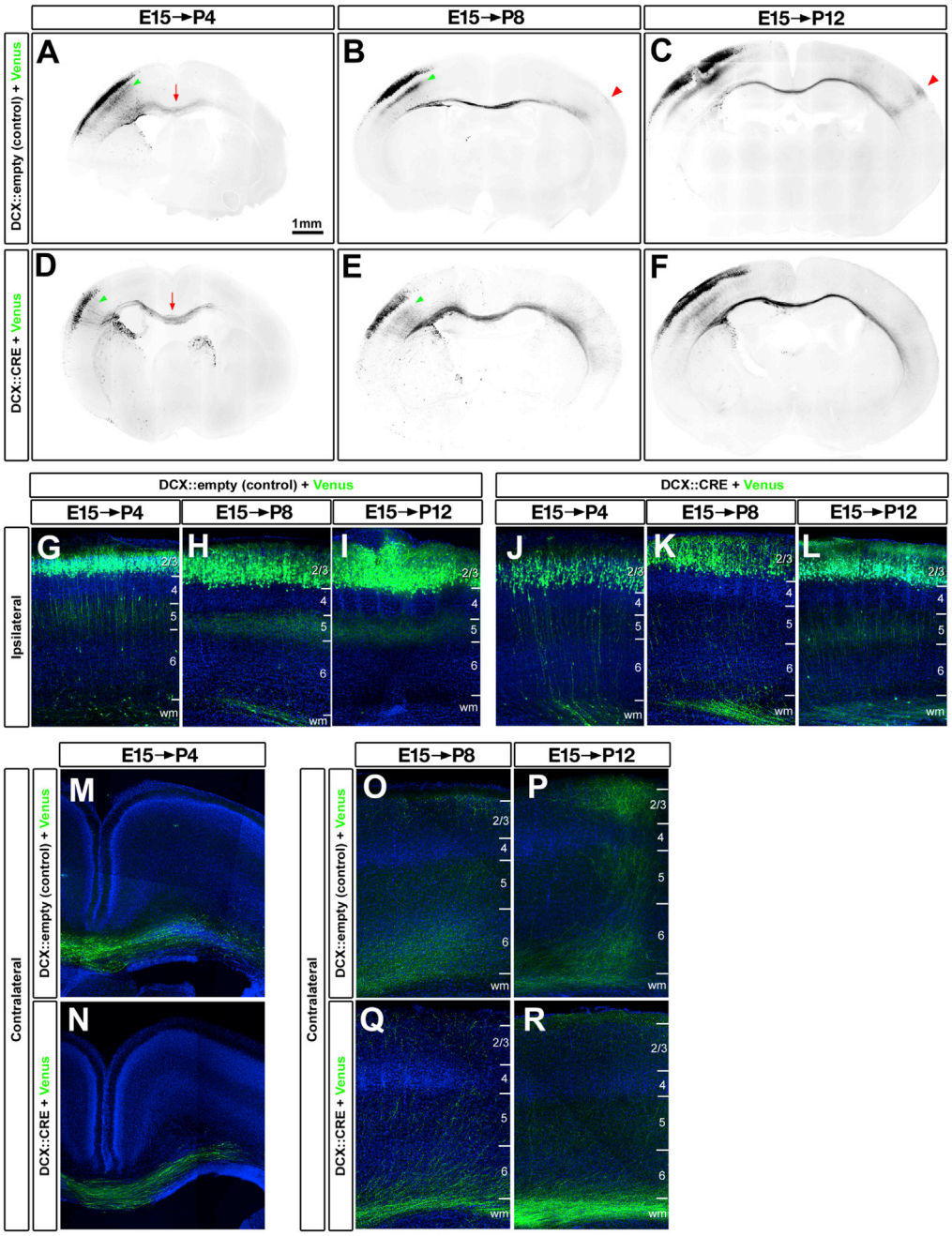

Figure S2. Consequences of LKB1 Deletion on Axon Growth and Branching In Vivo, Related to Figure 1

(A–F) Representative coronal sections of brains of *Lkb1* floxed mice upon electroporation of a control vector (A–C) or CRE coding plasmid (D–F). Mice were sacrificed at the indicated ages and slices stained with anti-GFP (inverted signal).

(G–L) Magnification of the ipsilateral side of A–F showing axon branching progression on cortical layer V with time in wild-type neurons (G–I) or reduced branching of Cre-electroporated neurons (J–L).

(M and N) Magnification of the contralateral side of A and D showing that axons have crossed the midline by postnatal day 4 in both control (M) and CRE (N) electroporated condition.

(O–R) Magnification of the contralateral side of B, C, E and F showing the development with time of terminal axonal branching of wild-type neurons (O–P) and its impairment in Cre-electroporated neurons (Q–R). Blue fluorescence in (G–R) is Hoechst 33342 staining.

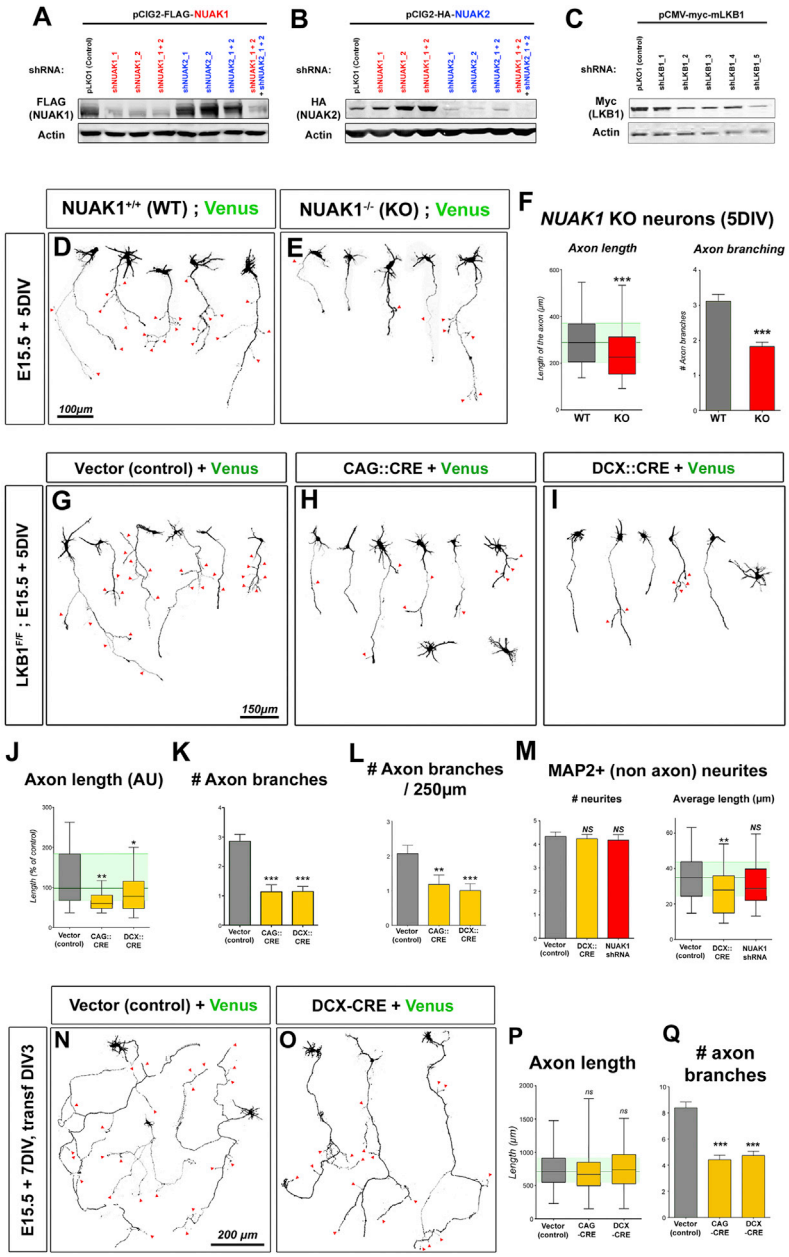

Figure S3. Genetic Loss of LKB1 or NUAK1 Disrupts Axonal Branching In Vitro and Is Not due to Delayed Polarization, Related to Figure 3

(A–C) Validation of shRNA targeting mouse *Nuak1* (A), mouse *Nuak2* (B) and mouse *Lkb1* (C) in HEK293T cells. shRNA targeting *Nuak1* are indicated in red and shRNA targeting *Nuak2* are indicated in blue. Western-blot analysis was performed with the indicated antibodies.

(D and E) Genetic loss of *Nuak1* leads to decreased axonal branching at 5 DIV.

(F) Quantification of axon length and branching upon genetic loss of *Nuak1* at 5DIV.

(G–I) Single cell deletion of *Lkb1* by Cre electroporation decreased axonal branching a 5DIV.

(J–L) Quantification of axon length (J), number of axon branches (K) or # of axon branches per 250 µm of axon (L) upon genetic loss of *Lkb1*.

(M) Loss of LKB1 or NUAK1 does not affect the number of MAP2 positive neurites at 5DIV, while only loss of LKB1 affects MAP2 positive neurite length.

(N and O) Representative *LKB1*$^{F/F}$ neurons transfected with a control (N) or CRE coding plasmid (O). E15.5 dissociated cortical neurons were transfected with Magnetofection after 3DIV and cultured for an additional 4DIV. Co-transfection with myristoylated Venus was used to determine neuron morphology.

(P and Q) Quantification of axon length (P) and number of axonal branches (Q) from neurons described in (N-O). Data represent 25th, 50th and 75th percentile (F, J, M) or average value ± SEM (F, K, L, M).

Statistical analysis: Mann-Whitney test. Data are a minimum of three independent experiments. (F) N_{WT} = 122, N_{LKB1} = 242. (J-L) $N_{control}$ = 175, $N_{CAG::Cre}$ = 98, $N_{DCX::Cre}$ = 167. (M) $N_{control}$ = 100, $N_{DCX::CRE}$ = 80, $N_{NUAK1\ sh}$ = 52. (P-Q) N_{Vector} = 55, $N_{DCX::Cre}$ = 60, $N_{CAG::Cre}$ = 75.

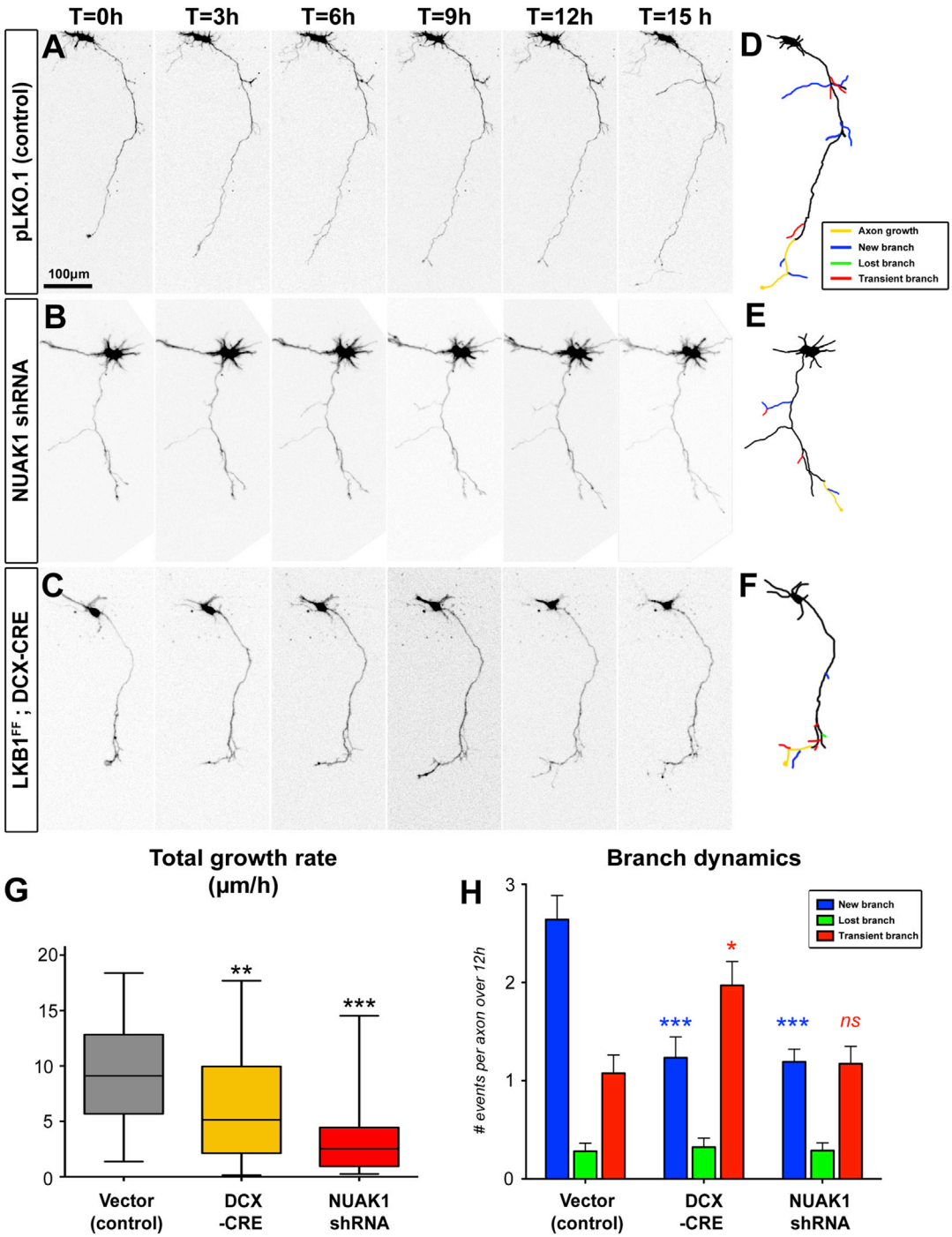

Figure S4. Dynamics of Axon Growth and Branching In Vitro in LKB1- or NUAK-Deficient Neurons, Related to Figure 3

(A–C) Progressive axonal changes of 5 or 6DIV cortical neurons electroporated at E15 with a control vector (A), shRNA targeting NUAK1 (B) or a CRE encoding plasmid (C) imaged for the indicated times. Neuron morphology was determined by co-electroporation of a Venus-encoding plasmid.

(D–F) Drawings of the axonal development of neurons shown in (A-C) over a 15 hr period. Colors indicate axon growth over 15 hr (yellow), creation of new branches that persist up to the end of the movie (blue), retraction of branches present at the origin of the movie (green) and the formation of new branches that retract before the end of the movie (red).

(G) Calculation of axon elongation rate of neurons in (A-C). Data represent 25th, 50th and 75th percentile.

(H) Average number (±SEM) of new, lost and transient branches of neurons shown in (A-C).

Statistical analysis: Mann-Whitney test. Data of (G-H) are a minimum of three independent experiments. $N_{control}$ = 40, $N_{DCX::Cre}$ = 35, $N_{NUAK1sh}$ = 52.

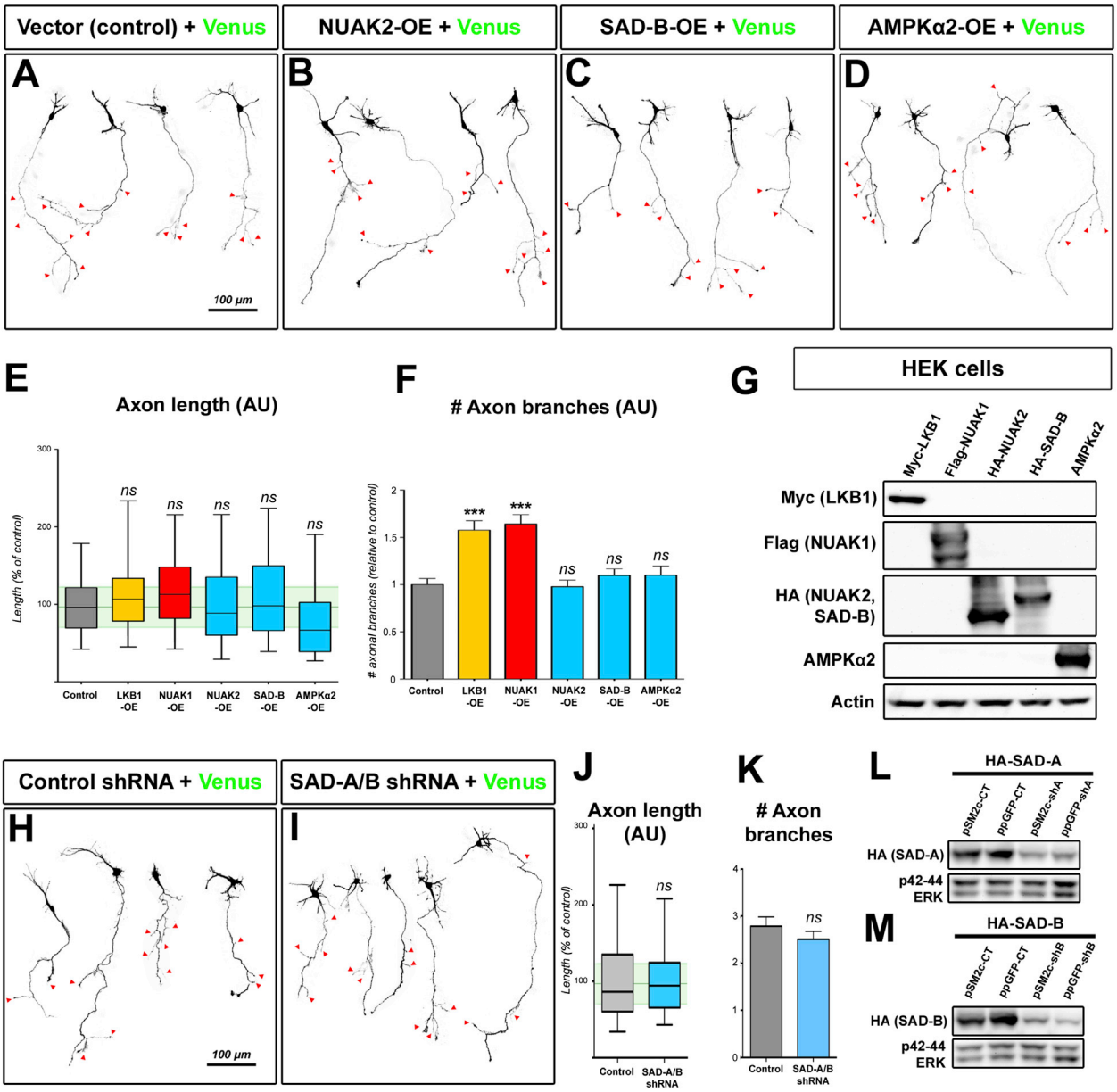

Figure S5. Overexpression of LKB1 and NUAK1, but Not Other AMPK-Like Kinases, Is Sufficient to Increase Axon Branching in Cortical Neurons, Related to Figure 3

(A–D) Representative neurons 5DIV after electroporation with plasmids encoding control (A), NUAK2 (B), SAD-B (C) or AMPKα2. Red arrowheads point to axon branches.

(E and F) Quantitation of axon length (E), and average number of collateral branches (F) for the conditions shown in (A-D). Data represent 25th, 50th and 75th percentile (E) or average value ± SEM (F).

(G) Validation of the expression of LKB1 and AMPK-related proteins in HEK293T cells. Western-blot analysis was performed with the indicated antibodies.

(H and I) Representative neurons 5DIV after electroporation of a control vector (H) or shRNA constructs targeting SAD-A and SAD-B (I). Red arrowheads point to axon branches. Neurons were electroporated with myristoylated Venus to assess neuron morphology. EUCE and cortex dissociation was performed at age E15.5.

(J and K) Quantification of axon length (J) and number of axonal branches (K) from neurons described in (H-I). Data represent 25th, 50th and 75th percentile (J) or average value ± SEM (K).

(L and M) Validation of shRNA against mouse *Sad-a* (L) or mouse *Sad-b* (M) in HEK292T cells. Western-blot analysis was performed with the indicated antibodies. Statistical analysis: Mann-Whitney test.

Data are a minimum of three independent experiments. (E-F) $N_{Control}$ = 89, $N_{LKB1\text{-}OE}$ = 82, $N_{NUAK1\text{-}OE}$ = 107, $N_{NUAK2\text{-}OE}$ = 116, $N_{SAD\text{-}B\text{-}OE}$ = 96, $N_{AMPK\ \alpha2\text{-}OE}$ = 63. (J-K) $N_{Control}$ = 69, $N_{SAD\text{-}A/B\ sh}$ = 88.

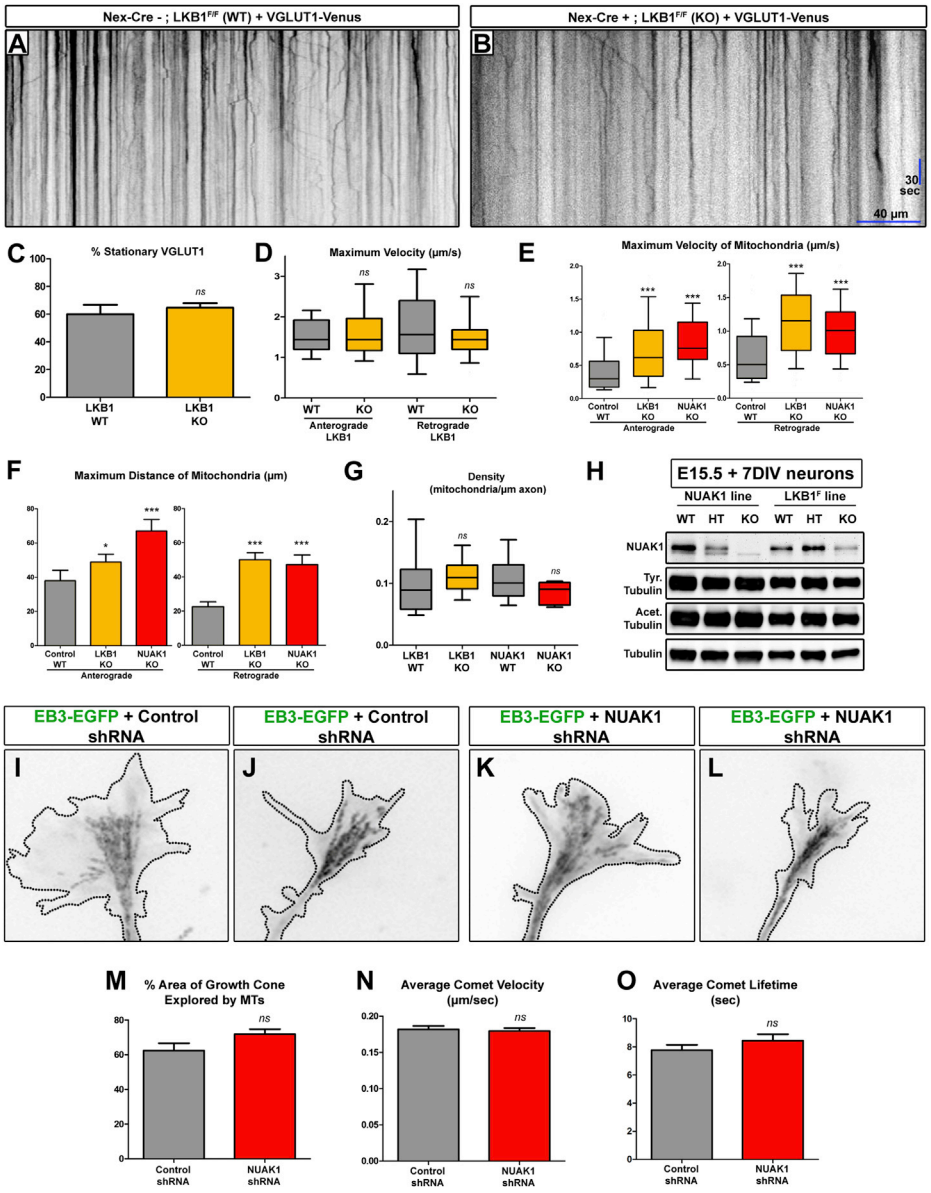

Figure S6. Presynaptic Vesicle Trafficking and Microtubule Dynamics Are Not Affected in the Axon Following Loss of NUAK1 Expression, Related to Figure 4

(A and B) Representative kymographs of VGlut1-Venus labeled presynaptic vesicles imaged every 750 ms for 3 min in dissociated neurons. Neuronal precursors from the indicated background were electroporated with VGlut1-Venus and HA-mCherry at embryonic day 15.5, then neurons were imaged at 7 DIV.

(C) The percentage of stationary VGlut1-positive presynaptic vesicles did not change upon loss of LKB1 (±SEM).

(D) Anterograde and retrograde maximum velocities of VGLUT1 vesicles were unaffected by the loss of LKB1 (25th, 50th, and 75th percentile).

(E) Maximum velocity increased for axonal mitochondria in both the anterograde and retrograde direction upon loss of LKB1 or NUAK1 (25th, 50th, and 75th percentile).

(F) Loss of LKB1 or NUAK1 also increased the maximum distance traveled by mitochondria in both directions (±SEM).

(G) Mitochondrial density along the axon was unaffected in LKB1 and NUAK1 knockout neurons at 5DIV (25th, 50th, and 75th percentile).

(H) Loss of LKB1 or NUAK1 does not change the relative abundance of tubulin, acetylated tubulin or tyrosinated tubulin in 7 DIV dissociated neurons.

(I–L) Representative maximum intensity projections of 5 min videos acquired from the growth cones of neurons expressing HA-mCherry and EB3-EGFP as wells as control shRNA (pLKO.1, I-J) or NUAK1 shRNA (K-L).

(M) Loss of NUAK1 does not affect the area of the growth cone explored by growing microtubules (±SEM).

(N and O) Loss of NUAK1 does not affect the average comet velocity (N) or the lifetime of EB3 comets (O) (±SEM). N numbers for (A-D): $N_{NexCre\ WT}$ = 271 VGLUT1 vesicles from 6 neurons, $N_{NexCre\ KO}$ = 250 VGLUT1 vesicles from 8 neurons. N numbers for (E-G) are the same as in Figure 5. N numbers for (I-O): $N_{Control\ shRNA^{+}EB3EGFP}$ = 228 comets from 20 growth cones, $N_{NUAK1\ shRNA^{+}EB3EGFP}$ = 218 comets from 21 growth cones.

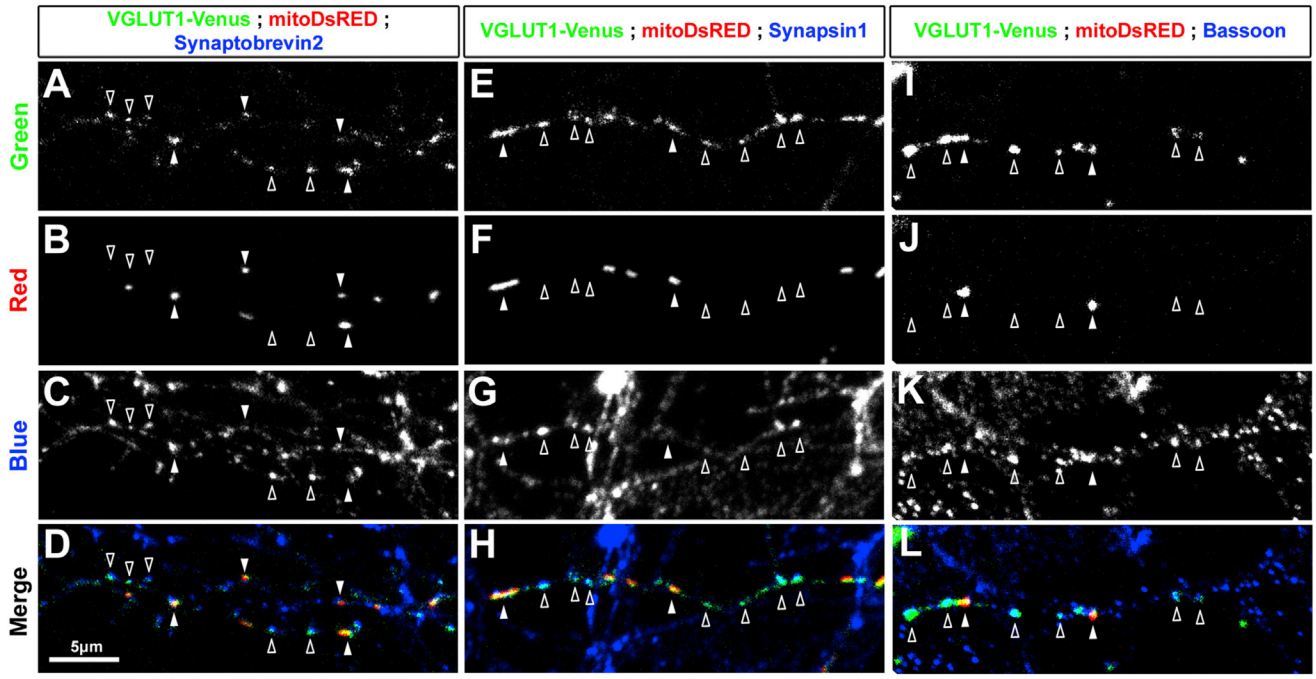

Figure S7. VGLUT1-Venus Puncta in the Axon of E15 Cortical Neurons Maintained for 7 Days in Culture Colocalize with Three Other Presynaptic Markers, Related to Figure 7

(A–L) Representative high magnification images of axon segments stained with antibodies against the presynaptic markers Synaptobrevin2 (A-D), Synapsin1 (E-H) or Bassoon (I-L). Cortical neurons were electroporated at E15.5 with plasmids encoding VGLUT1-Venus and mitoDsRed, then fixed at 7DIV. VGLUT1 puncta associated (filled arrowheads) or not associated with mitochondria (empty arrowheads) were detected by direct fluorescence of Venus and DsRED, respectively. Presynaptic markers were detected using immunofluorescence with the indicated antibodies. The vast majority of VGLUT1-Venus puncta co-localize with the three other presynaptic markers.